ICE, CLOUD, and Land Elevation Satellite
(ICESat-2) Project

Algorithm Theoretical Basis Document (ATBD)
for
Precise Orbit Determination, Orbit Design, and Geolocation Parameter Calibration

Prepared By:

Scott B. Luthcke
(NASA/GSFC, Code 698)

Teresa Pennington, Bryant D. Loomis
(SGT@NASA/GSFC, Code 698)

Tim Rebold, Taylor C. Thomas
(EMERGENT@NASA/GSFC, Code 698)

Goddard Space Flight Center

Greenbelt, Maryland

Suggested contents by releases

Preliminary ATBD (due Sept. 2012)

1.0 Introduction: *Short introduction of what this ATBD will cover. Covers a product, a parameter, ancillary processing, etc.*

2 - Overview and background information: *General description of the algorithm function in easily understandable terms that describes what it does, how it does it and any supporting or background information that makes it clearer. This section should provide information that the public affairs office can easily use for their release of information on ICESat-2/ATLAS.*

3 - Algorithm Theory. Clearly this is where much of the work over the next two years needs to be done. At this point, Section 3.0 can be very high level.

4 - Algorithm Implementation. This will also be a large part of the future work. At this point, the Input Parameters (Section 4.2) and Output Parameters (Section 4.3) is the most important part. We want to make sure the necessary parameters are being collected by ICESat-2, or from other sources.

ATBD content

All sections should be near final except section 6 on test data. Section 6 provide information as available.

ATBD final

All sections final based on ATLAS designed for algorithm implementation, testing and expected processing for at least the first year of mission. It should identify any expected tuning or calibrations that are expect to occur during the Mission verification/calibration phase (Commissioning phase?)

Abstract

Foreword

This document is an Ice, Cloud, and Land Elevation (ICESat-2) Project Science Office controlled document. Changes to this document require prior approval of the Science Development Team ATBD Lead or designee. Proposed changes shall be submitted in the ICESat-II Management Information System (MIS) via a Signature Controlled Request (SCoRe), along with supportive material justifying the proposed change.

In this document, a requirement is identified by "shall," a good practice by "should," permission by "may" or "can," expectation by "will," and descriptive material by "is."

Questions or comments concerning this document should be addressed to:

ICESat-2 Project Science Office
Mail Stop 615
Goddard Space Flight Center
Greenbelt, Maryland 20771

Preface

This document is the Algorithm Theoretical Basis Document for the TBD processing to be implemented at the ICESat-2 Science Investigator-led Processing System (SIPS). The SIPS supports the ATLAS (Advance Topographic Laser Altimeter System) instrument on the ICESat-2 Spacecraft and encompasses the ATLAS Science Algorithm Software (ASAS) and the Scheduling and Data Management System (SDMS). The science algorithm software will produce Level 0 through Level 4 standard data products as well as the associated product quality assessments and metadata information.

The ICESat-2 Science Development Team, in support of the ICESat-2 Project Science Office (PSO), assumes responsibility for this document and updates it, as required, as algorithms are refined or to meet the needs of the ICESat-2 SIPS. Reviews of this document are performed when appropriate and as needed updates to this document are made. Changes to this document will be made by complete revision.

Changes to this document require prior approval of the Change Authority listed on the signature page. Proposed changes shall be submitted to the ICESat-2 PSO, along with supportive material justifying the proposed change.

Questions or comments concerning this document should be addressed to:

Thomas Neumann, ICESat-2 Project Scientist
Mail Stop 615
Goddard Space Flight Center
Greenbelt, Maryland 20771

Review/Approval Page

Prepared by:

Scott Luthcke POD Lead NASA/GSFC Code: 698 Greenbelt, MD 20771	
Teresa Pennington Systems Engineer SGT Inc. @ NASA GSFC 7701 Greenbelt Rd, Greenbelt, MD 20770 Tim Rebold POD/PPD Engineer Emergent @ NASA GSFC 6411 Ivy Ln, Greenbelt, MD 20770 Bryant Loomis POD/PPD Engineer SGT Inc. @ NASA GSFC 7701 Greenbelt Rd, Greenbelt, MD 20770 Taylor Thomas Aerospace Engineer Emergent @ NASA GSFC 6411 Ivy Ln, Greenbelt, MD 20770	
Reviewed by: ?????	
Bea *<Enter Position Title Here>* *<Enter Org/Code Here>*	*Tom* *<Enter Position Title Here>* *<Enter Org/Code Here>*
Approved by: ????	
Thorsten *<Enter Position Title Here>* *<Enter Org/Code Here>*	

Change History Log

Revision Level	Description of Change	SCoRe No.	Date Approved
1.0	Initial Release		
5.0	Draft Version 5.0 completed 2/20/14		
6.0	Draft Version 6.0 completed 5/1/2015 – moving of interfaces and formats to a POD ICD document		

List of TBDs/TBRs

Item No.	Location	Summary	Ind./Org.	Due Date
1	2.0	L2 data product description		
2		Define Geolocation ATBD, Section(s) throughout document		
3	4.4.3 – 4.4.5	Input data formats to be completed in Appendix B		
4	4.5.1 – 4.5.3	Output data formats to be completed in Appendix B		
5	Table 4.7.3	Define time variable gravity		
6	Table 4.7.3	Define high resolution geoid		
7	Table 4.7.3	Define non-tidal loadings		
8	9.3.4.2	Complete Solid Earth Tides and Ocean Tides		
9	9.4.4.3	Define load tide correction degree and order		
10	9.4.4.6	Complete Atmospheric loading section		
11	9.4.4.7	Define section describing tidal frequencies		
12	Throughout	New time varying range bias calibration considerations need to be completely integrated within this document.		
13	6.0	Section 6.0 needs to be completed with ICESat-1 and current simulation performance assessment, as well as test data simulation plan and details and GRT and MRT testing support plan.		
14	Abstract	Complete Abstract		

Table of Contents

List of Figures

List of Tables

1.0 DOCUMENT SCOPE

Precision Orbit Determination (POD) is a complex multi-disciplinary problem that is at the core of geodetic satellite mission data analysis and product generation. Only a few institutes in the world have robust and mature software and expertise to meet ICESat-2's requirements. The ICESat-2 POD team is fully responsible for the software chosen, its implementation and modification, and its operational use and product generation and validation. The POD algorithms and methodologies are not intended to be software implemented by an independent group. Therefore, this document is not a traditional ATBD in that it does not attempt to document in detail the myriad of estimation, force and measurement modeling algorithms necessary to perform POD. More appropriately, this document focuses on the ICESat-2 specific POD implementation, requirements, as well as validation, pre-launch performance assessment, and mission and ground system testing support. However, Appendix A does contain a brief summary of the many algorithms necessary for ICESat-2 POD.

1.1 RELATED DOCUMENTATION

This section provides the references for this interface control document. Document references include parent documents, applicable documents, and information documents.

1.1.1 Parent Documents

Parent documents are those external, higher-level documents that contribute information to the scope and content of this document. The following ICESat-2 documents are parent to this document.

a) Ground System Requirements Document ICESat-2-GSPM-REQ-0330 ICESat-2
b) Algorithm Theoretical Basis Document (ATBD) for Global Geolocated Photons
c) ICESat-2-SYS_REQ-0450_GeolocationBudget_RevG.xlsx

1.1.2 Applicable Documents

Applicable documents include reference documents that are not parent documents. This category includes reference documents that have direct applicability to, or contain policies binding upon, or information directing or dictating the content of this document. The following ICESat-2, EOS Project, NASA, or other Agency documents are cited as applicable to this interface control document.

a) Algorithm Theoretical Bases Document (ATBD) for Precise Orbit Determination and Instrument Parameter Calibration
b) Algorithm Theoretical Basis Document (ATBD) for ATL03g ICESat-2 Receive Photon Geolocation

c) Algorithm Theoretical Basis Document (ATBD) for ATL03a Atmospheric Delay Correction to Laser Altimetry Ranges
d) Interface Control Document (ICD) Between the Science Investigator-led Processing System (SIPS) and Precision Orbit Determination (POD)/Precision Pointing Determination (PPD) – ICESat-2-SIPS-IFACE-1636
e) Mission Operation Center (MOC) Interface Control Document - 6145330000R0_A%2CMOCICD%2CCDRLMOCMO-2.pdf
f) ASAS Software Design Description Document ICESat-2-SIPS-SPEC-1621 (ATL02 File Format Definition)
g) ICESAT-2 Mission Operations Concept Document ICESAT-2-SYS-PLAN-0006

2.0 POD OVERVIEW AND CORE SOFTWARE

The geolocation of the laser altimeter surface return, or bounce point, relies on the precise knowledge of several components. These include the position of the spacecraft center of mass, the tracking point offsets of the instrument related to the spacecraft center of mass, the pointing of the instrument, and the altimeter range observations.

The parameters defining the temporal history of the spacecraft center of mass position and velocity, or the orbit, can be refined through the minimization of the spacecraft tracking data residuals utilizing precise tracking data measurement models. This precision orbit determination (POD) process is capable of estimating both dynamic parameters contributing to the force modeling of the spacecraft, and measurement modeling parameters which can include a host of geophysical parameters such as Earth orientation parameters, and tracking system specific parameters such as antenna phase center offsets. The accuracy of the precision orbit solution relies on the fidelity of the force and measurement models, and the quality of the tracking data.

The software program to be used in performing the ICESat-2 precise orbit determination is the GEODYN-II program, which evolved from the original GEODYN program that was developed at NASA GSFC in the 1960's. This current version of the software has been operational since 1985, and has been extensively used for satellite orbit determination, altimeter geolocation, geodetic parameter estimation, tracking instrument calibration, and orbit prediction, and is capable of handling essentially all types of satellite tracking data.

GEODYN-II has been utilized on every NASA geodetic Earth and planetary altimeter mission including TOPEX/Poseidon, Jason-1, Jason-2, Mars Global Surveyor, Shuttle Laser Altimeter I & II, ICESat, GRACE, Lunar Reconnaissance Orbiter, MESSENGER, and GRAIL. Of note is the use of the GEODYN-II program to achieve and confirm 1-centimeter radial orbit accuracy for Jason-1 [*Luthcke et al., 2003*].

Solution strategy can also contribute to the final orbit and geolocation accuracy. For example, the simultaneous processing of GPS and SLR tracking can provide a more accurate orbit solution than is possible with either tracking data type alone [*Rowlands, 1997*]. Similarly, the simultaneous estimation of altimeter instrument parameters, along with orbit and geophysical parameters, is a robust solution strategy for improved geolocation accuracy [**add reference**]. Therefore, the implementation of the estimation process must include the ability to perform simultaneous solutions for instrument, orbit and geophysical parameters through the reduction of a combination of instrument range and spacecraft tracking data observations.

The GEODYN-II precision orbit determination and geophysical parameter estimation program is equipped with a full set of Multi-Beam Laser Altimeter (MBLA) range data processing capabilities. The direct altimetry and dynamic crossover measurement model algorithms (Geolocation ATBD, Section ?), along with the classic geolocation algorithms (ATL03g ICEsat-2 Receive Photon Geolocation ATBD, Section 3.1), are fully implemented into the GEODYN-II software. GEODYN-II supports the simultaneous estimation of orbit and instrument measurement modeling parameters through the reduction of a combination of spacecraft tracking

and laser altimeter ranging data. The GEODYN MBLA processing capabilities are supported for both Earth orbiting and interplanetary laser altimeter missions. Additionally, the data corrections discussed in Section 4 are fully implemented within the GEODYN program for laser altimeter and tracking data reduction.

The orbit and parameter estimation problem is divided into two parts: (1) the orbit modeling or prediction problem, and (2) the parameter estimation problem. The solution to the first corresponds to GEODYN's orbit generation mode, which relies on Cowell's method of numerically integrating the orbit. The second part of the problem corresponds to GEODYN's data reduction mode, which is based on the solution to the orbit prediction problem, and utilizes Bayesian least squares statistical estimation procedure to optimally estimate the parameters. A brief overview of the GEODYN estimation and orbit modeling processes are provided in the following sections. For a more complete discussion of the GEODYN parameter estimation and orbit and measurement modeling algorithms please refer to [*Pavlis, et al. 1998*].

3.0 ICESAT-2 DESIGN ORBIT AND REFERENCE GROUND TRACKS

3.1 Overview

The POD team developed the ICESat-2 orbit with the initial requirements of: (1) a 92° inclination orbit for coverage of polar ice and sea ice while still producing orbit-crossings for altimeter cross-over observations, (2) a frozen orbit to limit altitude variation at any given latitude in order to maintain beam pattern geometry on the surface, (3) a ~91-day repeat to sample seasonal variation with a ~30-day near repeat for temporal sampling of sea ice, (4) low earth orbit for altimeter instrument radiometry considerations.

3.2 Orbit Design Procedure

The first step is to determine the number of nodal revolutions the satellite will complete by repeat, *N,* and the number of Earth rotations performed with respect to the satellite's orbital plane, *D* (nodal days). Generally the science requirements will constrain these numbers. Altitude requirements as well as track density (coverage) are typically known well enough to bound the ratio *N*/*D*.

Given a satellite's general altitude (semi-major axis) the period $\mathcal{P}$, of a satellite is expressed by Kepler's 3rd Law as:

$$\mathcal{P} = 2\pi\sqrt{\frac{a^3}{\mu}} \qquad (3.2.1)$$

where a is the satellite's semi-major axis and μ is the standard gravitational parameter for the Earth.

N orbit periods should be approximately equal to the *D* nodal days to repeat. Further insight can be gained from applying Bezout's Theorem (Pie, 2008) expressed below as:

$$d \cdot N - m \cdot D = k \qquad (3.2.2)$$

where *m* is the number of sub-cycle revolutions, *d* is sub-cycle nodal days, and *k* is the ground-track nodal spacing deviation (integer 1,2…).

The closest sub-cycles, $k = \pm 1$ for ICESat-1 were important orbit design factors where these 2 sub-cycles ended up dividing the satellite's 91 day repeat cycle into 3 nearly even periods where the ground-track nearly repeated itself.

Once *N* and *D* are selected we can begin a more refined analysis involving some of the Earth's gravitational field zonal terms. The analysis also requires as input a mean orbit inclination, i_0 that is typically determined from science or mission requirements. Again, the satellite's mean semi-major axis, a_0 can be initially estimated by calculating the period of the orbit and ensuring *N* orbit periods approximately takes *D* days to complete. We can then look over a range of mean semi-

major axis values centered about our initial estimate. With each mean semi-major axis a mean eccentricity, e_o can be computed to ensure that the orbit is properly frozen. Conditions for a frozen orbit are given as:

$$\dot{\omega} = 0 \, , \dot{e} = 0 \quad (3.2.3)$$

where secular rates for mean argument of perigee, $\dot{\omega}$ and mean eccentricity, $\dot{e}$ vanish. The condition for no secular eccentricity rate is satisfied by selecting mean argument of perigee, ω_0 = 90° or 270°.

To nullify the secular rate for mean argument of perigee we calculate a mean frozen eccentricity using the following equations below:

$$k = 3nJ_2 \left(\frac{R_e}{a}\right)^2 \left(1 - \frac{5}{4}f\right) \quad (3.2.4a)$$

$$C = -\frac{3}{2}n\left(\frac{R_e}{a}\right)^3 sini_o \cdot F \quad (3.2.4b)$$

$$\begin{aligned} F = {} & J_3\left(1 - \frac{5}{4}f\right) - \frac{5}{2}J_5\left(\frac{R_e}{a}\right)^2\left(1 - \frac{7}{2}f + \frac{21}{8}f^2\right)\ldots \\ & + \frac{35}{8}J_7\left(\frac{R_e}{a}\right)^4\left(1 - \frac{27}{4}f + \frac{99}{8}f^2 - \frac{429}{64}f^3\right)\ldots \\ & - \frac{105}{16}J_9\left(\frac{R_e}{a}\right)^6\left(1 - 11f + \frac{143}{4}f^2 - \frac{715}{16}f^3 + \frac{2431}{128}f^4\right) \end{aligned} \quad (3.2.4c)$$

$$e_0 = \frac{C}{k} \quad (3.2.4d)$$

where J_2, J_3, J_5, J_7, J_9 are the Earth's gravity field even and odd zonal harmonics, R_e is the mean equatorial radius of the Earth, $f = sin^2 i_0$ and mean motion, $n = \sqrt{\frac{\mu}{a^3}}$.

We now have a mean frozen eccentricity for a given mean semi-major axis and inclination. We can determine how well the orbit repeats by evaluating the following condition:

$$D \cdot \frac{2\pi}{\omega_\oplus - \dot{\Omega}} = N \cdot \frac{2\pi}{\dot{M} + \dot{\omega}}$$

or

$$D \cdot \left(\dot{\mathrm{M}} + \dot{\omega}\right) - N \cdot (\omega_{\oplus} - \dot{\Omega}) = 0 \qquad (3.2.5)$$

where $\omega_{\oplus}$ is the Earth's average rotation rate, and rates for mean anomaly, argument of perigee and right ascension of ascending node ($\dot{M}, \dot{\omega}, \dot{\Omega}$) are theoretically calculated using zonal coefficients as in Vallado, 2001 (9-38,9-40,9-42) and Roh et al., 2009 to account for the odd zonal harmonics added to $\dot{\omega}$.

In addition, the orbital period given in terms of general orbit perturbations can be expressed as:

$$\mathcal{P} = \frac{2\pi}{\dot{\mathrm{M}} + \dot{\omega}} \qquad (3.2.6a)$$

With each orbit the resulting ground-track shift in longitude, $\Delta\lambda$ is given as:

$$\Delta\lambda = \mathcal{P} \cdot (\omega_{\oplus} - \dot{\Omega}) \qquad (3.2.6b)$$

Given *N* longitude shifts, we should arrive back to where we first started for the orbit to be qualified as an acceptable repeat candidate.

We can evaluate these conditions (equations 3.2.5 & 3.2.6) for every value of mean semi-major axis in our search interval and its corresponding frozen eccentricity. The pair of values that gives us the best repeat conditions is selected as the initial estimates of mean orbital elements with $\omega_0 = 90°$ or $270°$. We can also validate the frozenness of our orbit by inspecting the value calculated for $\dot{\omega}$. We expect that this value will be relatively small given the calculated frozen eccentricity.

We can next convert these mean elements into osculating elements using a GEODYN utility program called C2GMEAN. The osculating elements are used to generate an orbit in GEODYN that includes a larger gravity field expansion (70x70). Additionally, in the GEODYN runs the non-conservative forces are turned off, as well as Earth nutation, precession and polar motion. Earth rotation is fixed to a constant rate (mean over the time period of the mission).

Due to the higher gravity terms we expect to lose the repeat ground-track and lose some of the frozen orbit characteristics. We wish to adjust the mean semi-major axis and eccentricity to achieve repeat and frozen orbit conditions again with this more detailed geopotential model. We can use an optimization procedure to adjust these mean values until the ground-track closure at repeat is within a suitable tolerance and the altitude variation of the orbit has been effectively minimized. A frozen orbit is essentially an orbit with minimal orbital element variation and this leads to minimum altitude variation among each orbit pass. The optimization procedure continuously changes between adjusted mean orbital elements and new osculating elements to start the next GEODYN simulation. The procedure iterates until a successful repeat-frozen orbit has been designed.

3.3 Tuned Orbit and Reference Ground Track

In addition to the orbit design considerations discussed above, the orbit Reference Ground Track (RGT) is tuned to pass through the center of the monthly narrow survey of ICESat-1 Track 412 near Summit Camp, Greenland (lat., lon., tolerance: 72.61319, -38.54596, 0.25 km).

The final tuned orbit parameters are shown in Table 3-1. The 91-day repeat orbit has sub-cycle near repeats at 29 and 62 days (Figure 3-1). The frozen design orbit altitude variation with respect to the ellipsoid and the altitude variation as a function of latitude are shown in Figure 3-2 and Figure 3-3. Frozen orbit performance metrics as in Roh et al., 2009 are shown in Figure 3-4.

The WGS84 ellipsoid is used:

a_e = 6378137 m (semi-major axis)

f_{inv} = 298.257223563 (inverse flattening)

The ICESat-2 RGT (mission elapsed seconds, latitude, longitude and height) has been computed using the final tuned design orbit and the intersection with Earth surface topography modeled using GMTED 2010 30 arcsec elevation with respect to EGM96 and then related to WGS84 ellipsoid, and CLS-CNES 2011 Mean Sea Surface. There are 1387 orbit tracks, where track 1 starts ascending just west of Greenwich.

Table 3-1 ICESat-2 Frozen Repeat Orbit

Mean Elements	Osculating Elements
a = 6855.9539 km	a = 6846.3943 km
e = 0.001398	e = 0.003269
i = 92°	i = 92.0013°
Ω = 0°	Ω = 0.1150°
ω = 90°	ω = 89.7978°
M = 180°	ω = 89.7978°
Repeat Orbit	
N revs = 1387	D = 91 nodal days (90.8193 days)
Design Metric Performance 1: 0.003719 m repeat ground-track offset Design Metric Performance 2: 104.4921 m altitude variation	

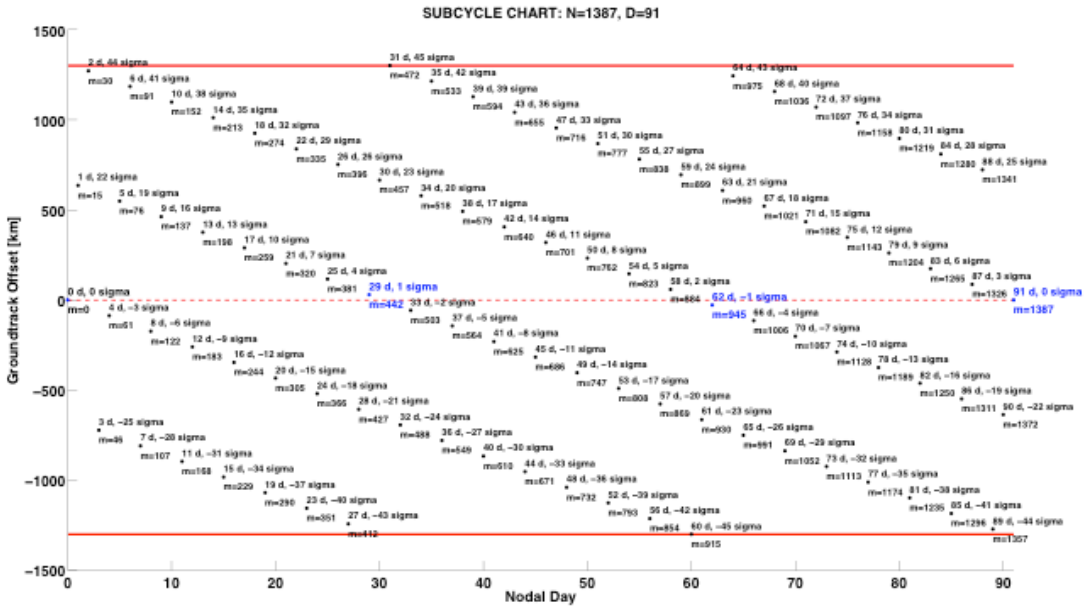

ICESat-2 Orbit Repeat Sub-cycle Chart: m is the number of orbit revolutions, sigma is nodal spacing = 2π/N = 28.893 km, 90.8193 days to repeat

Figure 3-1 ICESat-2 Repeat Sub-cycle Chart

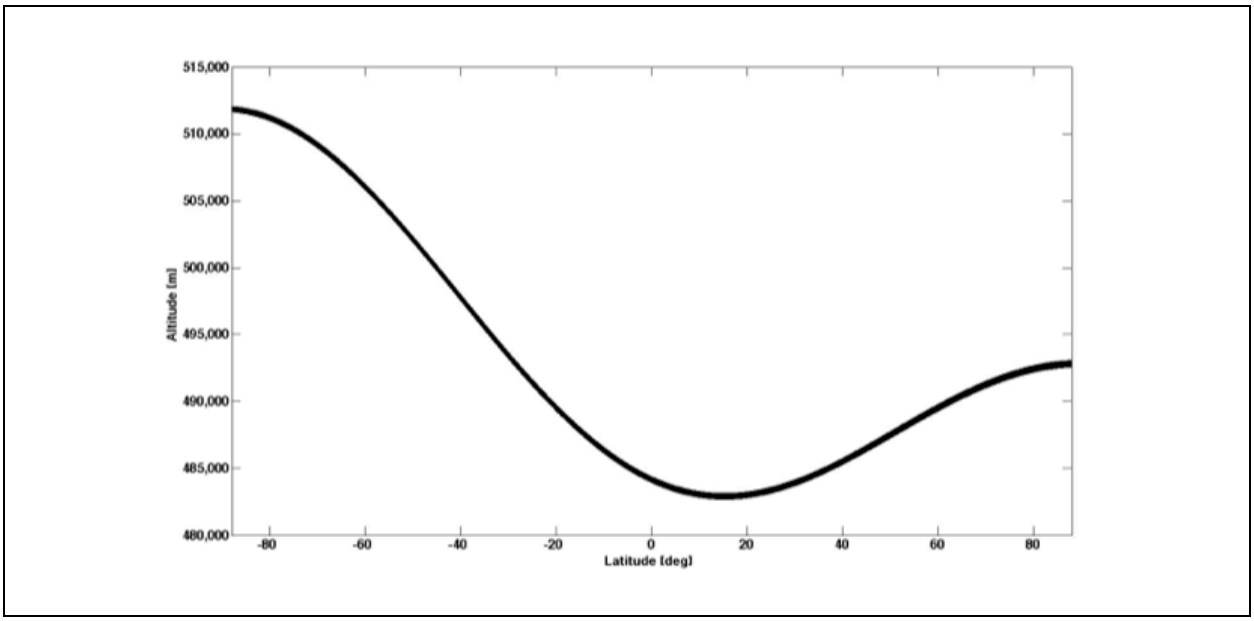

Figure 3-2 ICESat-2 Design Orbit Altitude with Respect to the Ellipsoid

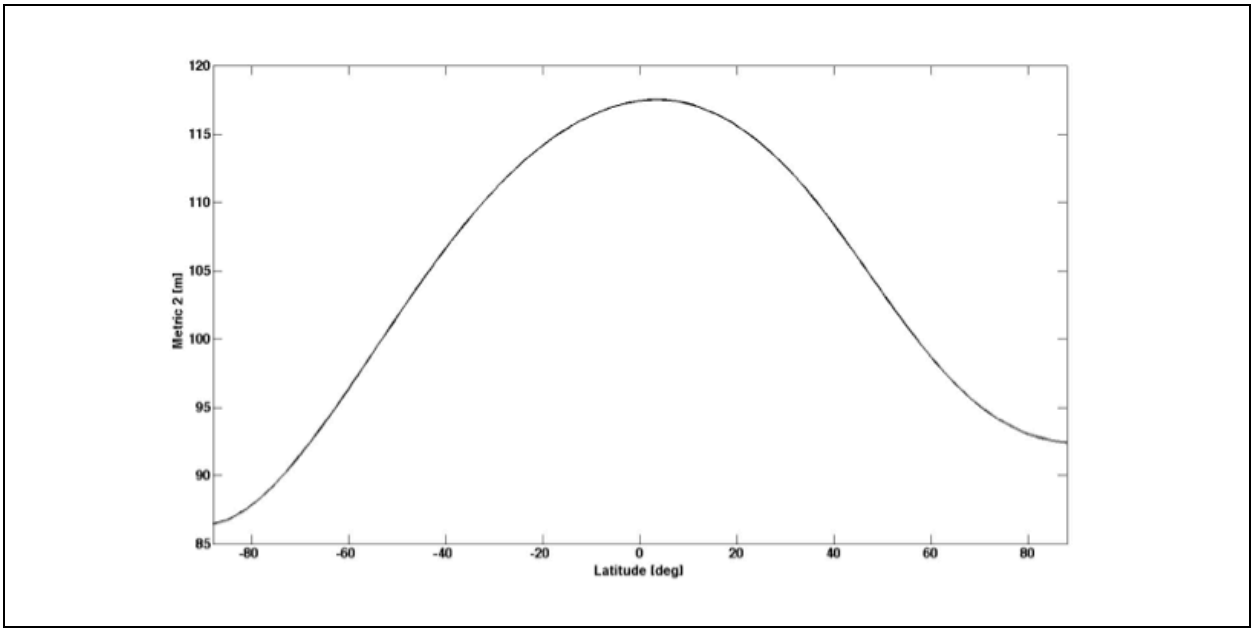

Figure 3-3 ICESat-2 Frozen Design Orbit Altitude Variation as a Function of Latitude

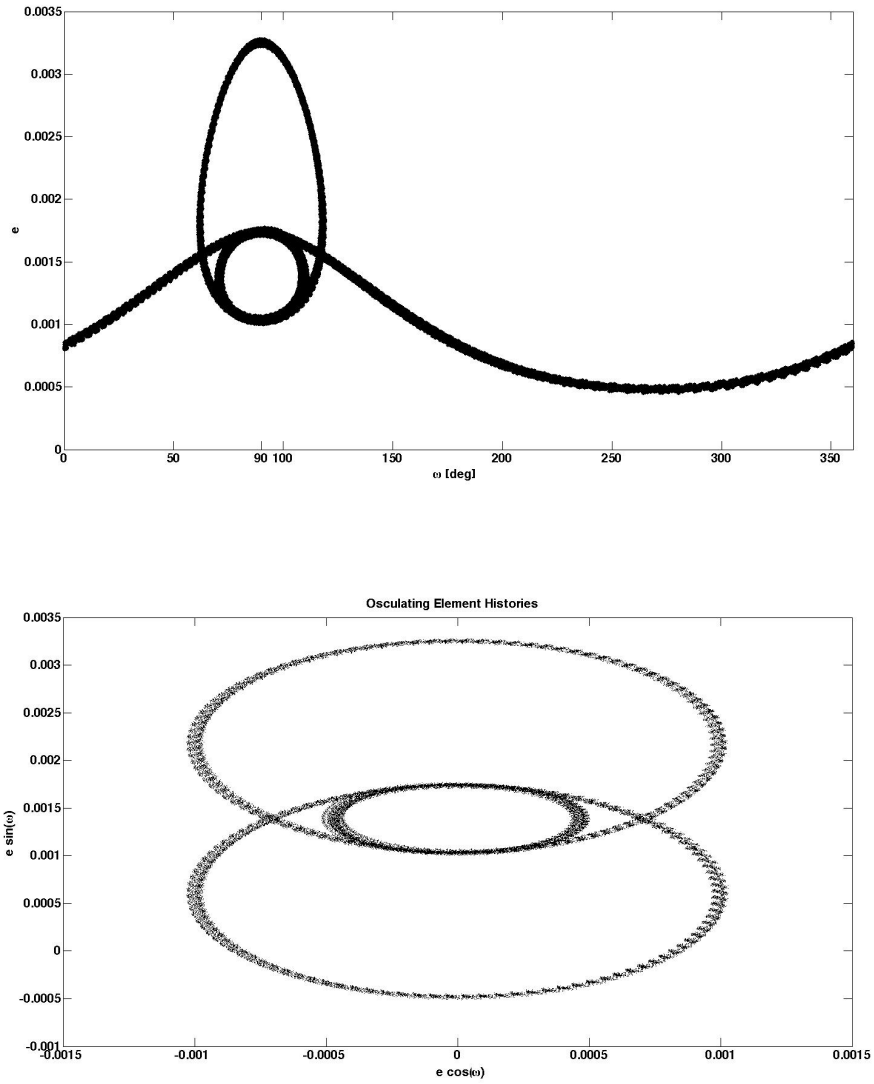

Frozen orbit performance metrics represented by osculating eccentricity vs. argument of perigee (as in Roh et al., 2009).

Figure 3-4 Frozen Orbit Performance Metrics

4.0 ICESAT-2 POD IMPLEMENTATION

4.1 Requirements

The ICESat-2 POD element requirement identified in the ICESat-2-SYS_REQ-0450_GeolocationBudget_RevG.xlsx document states that the Final POD Along and Cross-Track Error should be 20 cm 1σ RSS. This is given in the table below along with other POD requirements.

Table 4-1 ICESat-2 POD Requirements

Requirement	Details
Reference Ground Tracks (RGT)	ICESat-2 orbit design RGT design and simulation Pre-launch for PDR and CDR, as needed
Final POD	20 cm 1σ RSS Along and Cross-Track; 3 cm 1 σ Radial over 24-hr time interval Orbit position and velocity at 10 second rate 21 days after time stamp of data
Rapid POD and Predicted Orbit	48 hours after time stamp of data
ICRF-to-ITRF Quaternions	48 hours after time stamp of data
GPS-UTC, GPS Time Tag Correction	As required, and within 48 hours
Planetary Ephemeris	Updated as required
PPD Calibration	Within 2 weeks of Final PPD receiver Frequency as determined by analysis
Time-Varying Range Bias Calibration	For beams not monitored by the transmitter echo Performed on a 10 day basis or as determined by analysis Within 1 month of final POD/PPD

4.2 Heritage and Differences from ICESat-1

4.2.1 Heritage

The majority of the algorithms and software systems used for the ICESat-2 POD are heritage from ICESat-1. Updates required for the algorithms and software systems are noted in Table 4-2. The items listed below are only those that impact the POD element, and are a general summary. More detail can be found in Section 5.7.

Table 4-2 Heritage/Differences

ICESat-1	ICESat-2	System Development Consideration
600 km orbit, ICESat-1 S/C, COM	semi-major axis = 6855.9539 km (483 -512 km altitude), ICESat-2 S/C, COM	Force modeling; parameter estimation; POD strategy; COM modeling; improved overall measurement and force modeling.
GPS Blackjack Receiver/Antenna	RUAG Receiver/Antenna	Measurement modeling; observation correction; antenna modeling
SLR RR	SLR RR	Tracking scenarios for SLR RR; optical center variation
Altimeter and SRS 1 beam Analog waveform	New altimeter and LRS design 6 beams Photon counting	New altimeter measurement modeling and corrections. New calibration approach for combined pointing and range bias calibration.

4.2.2 Differences

These updated requirements are based primarily upon the differences between the ICESat-1 and ICESat-2 spacecraft. There are differences between the two spacecraft that have been identified as issues and/or concerns. These identified areas requiring updates to algorithms and software systems are outlined in Table 4.3.

Table 4-3 Spacecraft Differences Requiring Updates to Algorithms & Software Systems

Difference from ICESat-1 to ICESat-2	Impact	Approach
New GPS Receiver and Antenna	Data ingest and interpretation	Pre-launch receiver test data analysis
	Biases and Corrections	Pre-launch receiver test data analysis
	Tracking Stability	Pre-launch receiver test data analysis

	Antenna variation modeling and performance	Pre-launch receiver test data analysis and post-launch tuning
Lower Altitude Orbit	Force modeling improvements	Box-wing model based on pre-launch spacecraft material/optical properties. Tuned on-orbit. Reduced dynamic solution technique
Center of Mass (CoM)	New modeling Evaluation of errors which will directly impact elevation observations On-orbit calibration	
Photon Counting Altimeter	Surface detection algorithm, especially signal to noise during calibrations Surface property dependence and penetration Impact on time-varying pointing and range bias calibration	
Unobserved high-frequency motion of instrument pointing components	Jitter LTR motion LRS side relative alignment Impact on time-varying pointing and range bias calibration	
LRS moved to star-side	Significantly less number of stars tracked SST observations will be used by PAD to generate attitude solution with high accuracy in the regions where LRS have no star observation Continuous attitude solution will be provided during the sun-blinding with reasonable accuracy Quality of attitude solution is dependent on the actual change in the alignment between LRS and SSTs Impact on time-varying pointing and range bias calibration	

4.3 POD/PPD Element and POD Architecture

4.3.1 POD/PPD Element

The ICESat-2 mission structure is arranged such that all POD processing activities will occur within the larger POD/PPD element. In addition, the POD is required within the mission structure to interface with the MOC and the SIPS. The details of the POD/PPD-related project interfaces are documented in the MOC, the SIPS and the POD Interface Control Document (ICD) documents. The POD/PPD element data flow is summarized in Figure 4-1.

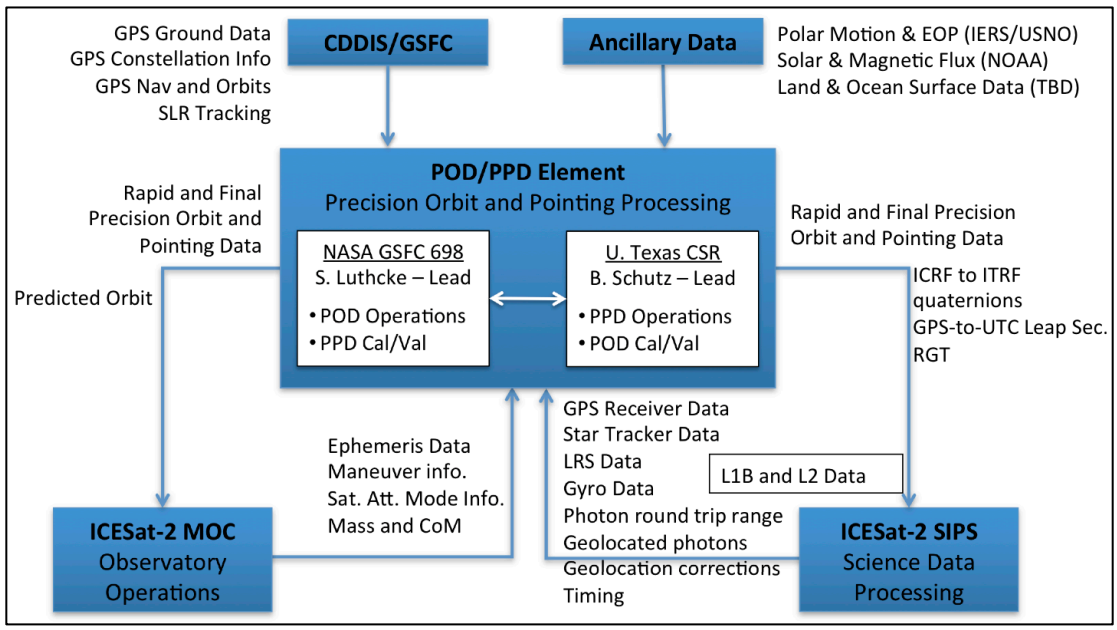

Figure 4-1 POD/PPD Element

4.3.2 POD Architecture

The POD element processing activities and architecture are further outlined in Figure 4-2. The POD Precision Geolocation System (PGS) is implemented on UNIX platforms. The robust PGS system is comprised of software modules written in PERL, UNIX, FORTRAN and MATLAB. The modular design of the system lends itself to ease of portability, modifications and updates.

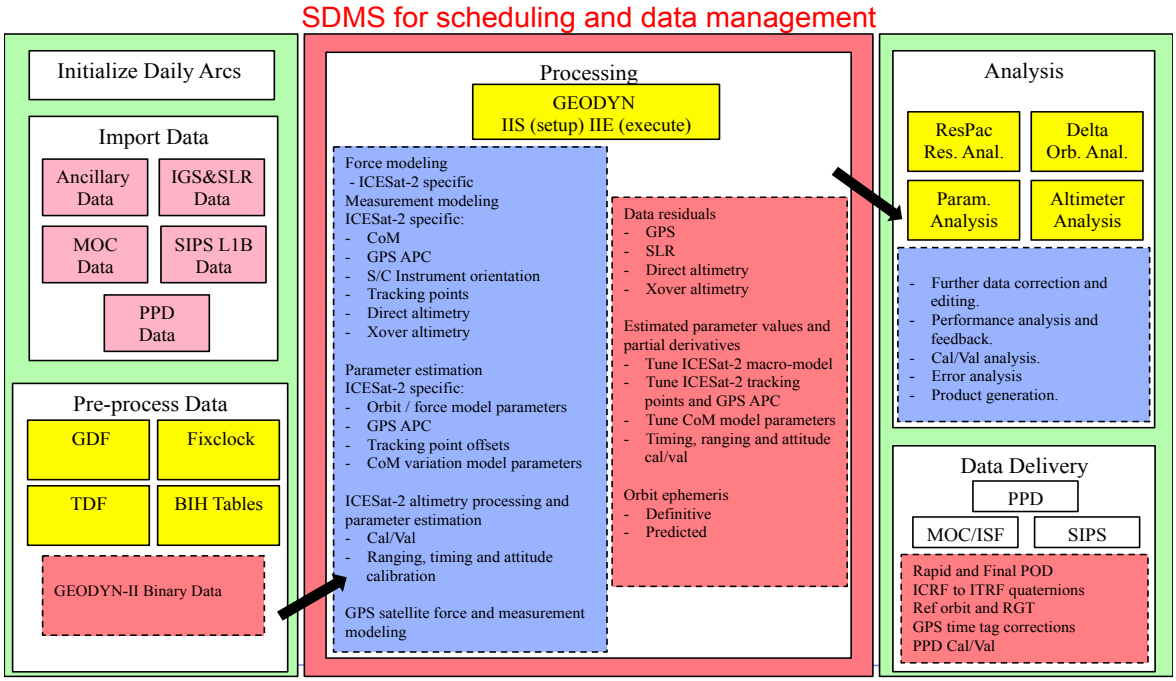

Figure 4-2 POD Precision Geolocation System (PGS) Architecture

4.4 POD Processing Timeline

The POD element is required to produce both rapid and final precise orbit determination products along with other supporting products. The POD processing timeline starting at 0 hours of the time stamp of the LIB data received are provided in Figure 4.3.

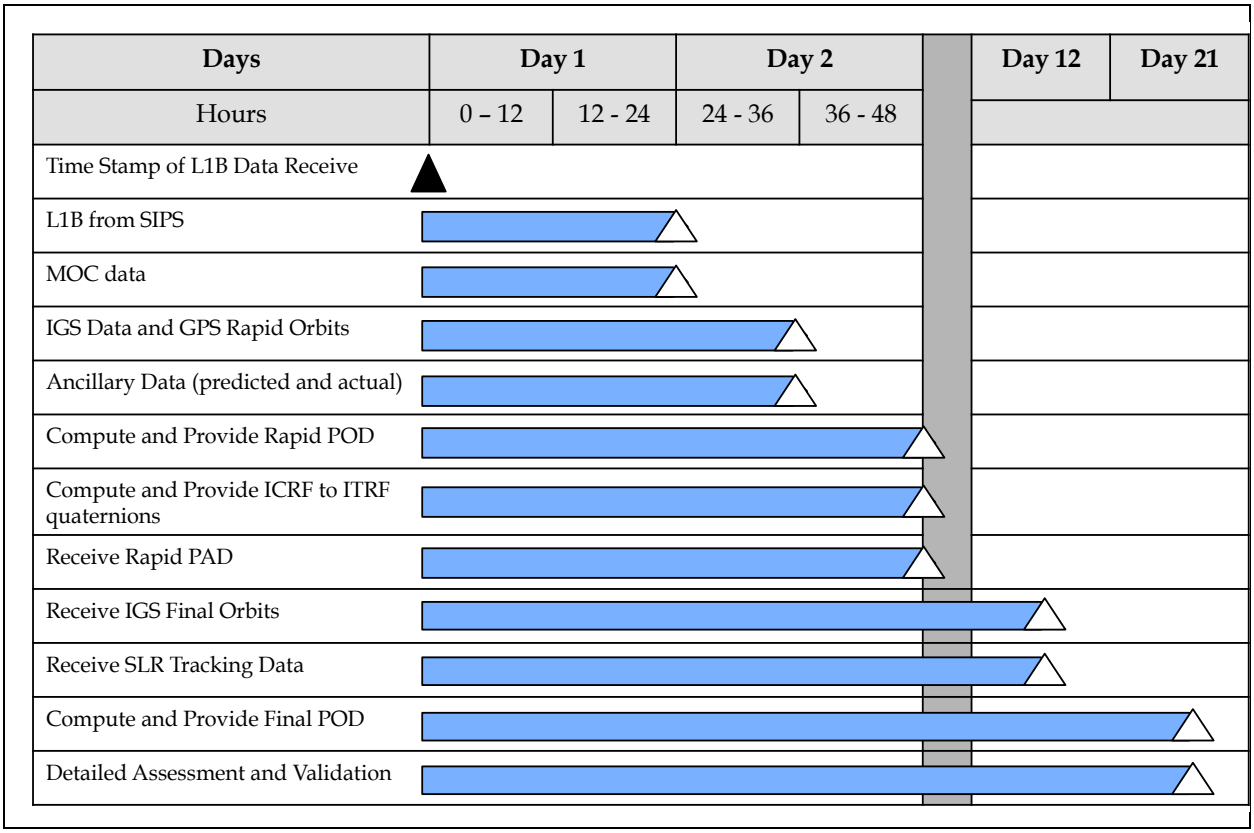

Figure 4-3 POD Processing Timeline

4.5 Observables, Models, Constants and Standards

Described in the tables that follow are the current set of proposed models, standards and constants. It should be noted that several of these will change over the next several years leading to launch, and may in fact change during the mission for various reprocessing. Tables 4-4 through 4-6 provided below are intended to capture the current state, and will be updated as needed.

Table 4-4 ICESat-2 Specific Models and Observables

Description	Model	Comment
ICESat-2 Observatory Force Model		
Non-conservative force model	Panel model developed based on pre-launch geometry and observatory surface optical properties. Tuned on orbit for the radiative	e.g. Luthcke et al. 2003, Luthcke et al. 1997, Marshall and Luthcke 1994. Calibration

	force model component. Geometry used for drag computations.	(tuning) discussed in Section 5.
ICESat-2 Observatory Measurement Models		
GPS antenna phase center offset vector and phase center variation map	Pre-launch measurements and tuned on-orbit	Luthcke et al. 2003. Calibration (tuning) discussed in Section 5.
SLR Retro-Reflector optical center offset vector	Pre-launch measurements and tuned on-orbit	
Center of Mass vector	Pre-Launch model from OSC. Model is function of SA orientation and fuel depletion, and delivered to POD team from OSC. Model parameters tuned on orbit.	
ICESat-2 Attitude	Telemetered ADS quaternions and SA drive angles	
GPS antenna RHC phase rotation corr.	Phase wind-up applied	[Wu et al., 1993]
GPS Tracking Data Observables		
Preprocessing	Conversion to RINEX-II/III format, fixclock, cycle slip detection and removal; detection and removal of bad GPS	Need telemetered data to RINEX-II/III conversion
Basic Observable	Ionosphere-free carrier phase and pseudo range observables. Corrected for 1st order by forming ionosphere-free linear combination.	
Modeled observables	Double-differenced carrier phase with ionosphere-free linear combination applied. Ability to form undifferenced and single-difference observables, if desired.	[Luthcke et al. 2003]
SLR Tracking Data Observables and Measurement Models		
SLR ranging observations	ILRS Normal Point data, station biases and other parameters from SLR analysis from several geodetic satellites.	[Luthcke et al. 2003, Lemoine et al. 2010].
Altimeter Observable and Measurement Models		
Modeled Observable	Direct altimetry – round trip range of photon Dynamic Crossover	Measurement models detailed in Appendix A. [Luthcke et al., 2002 & 2005]
Zero range point vector	The instrument team will measure the mean and develop a model of the variation as a function of temperature. The mean vector	*A priori* from instrument team.

	and variation model will be delivered to the POD team.	Calibrated on-orbit by POD team. See Section 5 concerning the calibration and validation details.
Atmospheric range delay	Three-dimensional atmospheric ray tracing with global meterological field.	ICESat-2 atmospheric range delay ATBD in development by Petrov and Luthcke

Table 4-5 GPS and SLR Models

Description	Model	Comment
GPS Satellite Force Modeling		
Non-conservative force model	Adjustable box-wing solar radiation pressure model (TUMSOL) Earth shadow model: conic model with oblate Earth, umbra and penumbra Earth albedo: TUM Attitude model: see GPS Attitude model in GPS Satellite Measurement Models section below	[Rodriguez-Solano, 2012] [Rodriguez-Salona, 2009] [Kouba, 2009]
GPS Satellite Measurement Models		
GPS satellite center of mass correction	Phase center offsets	igs.snx
GPS satellite antenna phase variations	PCV model with respect to phase center	igs08.atx
GPS Attitude model	GPS satellite yaw attitude model for nominal periods Yaw-attitude model for eclipse periods, applied based upon nominal yaw rates (See Section 9.4.2.4 of Appendix A) Reverse kinematic solution to provide alternative yaw-attitude solution during eclipse periods when Kouba's model may	[Bar-Sever, 1996] [Kouba, 2009; Kouba, 2013]

Description	Model	Comment
	be inaccurate. (See Section 9.4.2.5 of Appendix A)	
RHC phase rotation correction	Phase center wind-up	[Wu et al., 1993]
Satellite Clock Corrections	For Undifferenced and Single Differenced Observables	
GPS Ground Station Measurement Models		
GPS ground station network	Selection of best performing stations with best geographic coverage (selected from list of 91 "core" stations and alternate stations). Positions, velocities and discontinuity list from IGS (See Section 9.4.2.6 of Appendix A)	IGb08.snx (updated ITRF realization of ITRF2008) IGb08_core.txt soln_IGb08.snx
Station Marker -> antenna ARP eccentricity	dN, dE, dU eccentricities applied	igs.snx
Ground antenna phase center offsets and corrections	PCV model applied Receiver antenna and radome types	igs08.atx igs.snx
Atmospheric Path Delay (troposphere)	Line-of-sight delay expressed as a function of four zenith delay parameters scaling mapping functions. The four parameters are: hydrostatic zenith delay (computed), wet zenith delay, and N and E horizontal gradient. The mapping functions are: hydrostatic, wet, and gradient. Wet scale parameter estimated ~hourly and gradient scale parameters estimated ~daily.	IERS2010 Chen and Herring (1997) gradient mapping function. VMF1 hydrostatic and wet mapping function (Boehm et al. 2006a) as primary. GMF hydrostatic and wet mapping function (Boehm et al. 2006b) as secondary.
Ionosphere	1st order effect: removed by LC combination Higher order dispersive effects may be modeled	IERS2010
Gravitational Delay	Gravitational delay due to Earth modeled (see Section 9.4.2.7 of Appendix A)	IERS2010, Eq. (11.17)
SLR Ground Station Measurement Models		
Station positions and velocities	Consistent with ITRF2008	ITRF2008-TRF-ILRS.SNX

Description	Model	Comment
Station eccentricities	From ILRS ecc_xyz.snx	ILRS
Atmospheric propagation delay (troposphere)	Zenith Delay model Mapping Function for line-of-sight elevation dependence correction	[Mendes and Pavlis (2004)] [Mendes et al. 2002]

Table 4-6 POD General Models Constants and Standards

Description	Model	Comment
General Force Models		
Geopotential	eigen-6c.gfc_20080101_do_200.grv --- GM = 398600.4415 km**3/sec**2 --- AE = 6378.1366 km	Consistent with EIGEN6C
Time variable gravity	Contribution from atmosphere, non-tidal oceans, hydrology and ice. TBD… developed from GRACE analysis and/or models	Luthcke et al., 2013
Tidal	Solid earth tide: IERS2010 --- Ocean tide model: -GOT4.8 for short-period (< 1.2 cpd) -Self consistent equilibrium for: Node, Sa, Ssa -TPXO8 for Mm, Mf and Mt	IERS2010 Ray 1999
Solid Earth and Ocean Pole Tide: the centrifugal effect of polar motion.	$\Delta\bar{C}_{2,1} and\ \Delta\bar{S}_{2,1}$ corrections Correction is a function of wobble parameters (m_1, m_2) which are related to the polar motion variables (x_p, y_p)	IERS2010
N-body	Sun, Moon and all planets	JPL DE403 (or update)
Atmospheric Drag	MSIS for atmospheric density	[*Hedin*, 1987]

Description	Model	Comment
Earth Albedo	Modeled	[Knocke et al.,1988]
Relativistic corrections	Schwarzschild term (acceleration due to point mass of Earth) – secular drift in argument of perigee Lense-Thirring and de Sitter terms (geodesic precession) - precession of the orbit plan	IERS2010
Numerical Integration	Cowell predictor-corrector Fixed and variable step Equations of motion and variational equations.	GEODYN Implementation
Estimation Method	Partitioned Bayesian least squares	GEODYN Implementation
General Reference Frame and Constants		
Time System	GPS time given by receiver 1PPS and corrected based on position solutions.	
Conventional Inertial System	J2000 S.I. units Geocentric; mean equator and equinox of 2000 Jan 1.5 (J2000.0)	IERS2010
Precession – Nutation	IAU 2000A Precession-Nutation Model	[Coppola et al., 2009]
Planetary Ephemerides	JPL DE403 or DE411, etc…	[Standish et al., 1995]
Earth Orientation Parameter (EOP) Model	IERS 08 C 04 IERS 2010 Conventions for diurnal, semidiurnal, and long period tidal effects on polar motion and UT1.	IERS2010
UT1-TAI	IERS 08 C 04	IERS2010
Terrestrial Reference Frame	ITRF2008 reference frame realized through the set of station coordinates and velocities given in the IGS internal realization IGb08.snx	

Description	Model	Comment
Constants Defining Reference Ellipsoid for Geometric and Dynamic Calculations	$a_e = 63781337\ m$ $GM = 398005\ x\ 10^8\ m^3 s^{-2}$ $(\bar{C}_{2,0})_{JGM-2}^{tide-free} = -484.1654767\ x\ 10^{-6}$ $\omega = 7292115\ x\ 10^{-11}\ rad/s$	These defining constants were used to evaluate the derived constants according to *Moritz* [1984]
Derived Ellipsoid Constants	$(J_2)_{NASA,DMA}^{zero} = -(\bar{C}_{2,0})_{JGM-2}^{tide-free} * \sqrt{5}$ ... $... - 0.3 * (-3.11080\ x\ 10^{-8})$ $\frac{1}{f} = 298.257223563$ $\gamma_e = 9.79828685\ m/s$	$(J_2)_{\text{NASA/DMA}}^{zero}$ assumed k_2 = 0.3 In GEODYN, flattening is used only to calculate rectangular coordinates for the tracking stations when geodetic coordinates are given, in defining the sub-satellite location for altimeter data, and in calculating the geodetic altitude for drag purposes
High-resolution Geoid	EGM2008 mean tide system	WGS-84 referenced
Land Topography	GMTED2010 30 arcsec	
Ocean Mean Topography	CLS-CNES 2011	CNES
Surface Displacement for Stations and Altimeter Bounce Points		
Tidal	Solid earth tide: IERS 2010 Conventions --- Rotational deformation or solid Earth pole tide loading --- Ocean pole tide loading --- Ocean tide loading for land: -GOT4.8 for short-period (< 1.2 cpd) -Self consistent equilibrium for: Node, Sa, Ssa -TPXO8 for Mm, Mf and Mt Above is used to generate ocean loading amplitudes and phases using SPOTL (D. Agnew) --- Ocean altimeter return correction:	IERS2010 IERS2010 IERS2010, Desai 2002 Ray, 1999, IERS2010

Description	Model	Comment
	Combined ocean tide model and loading correction from: -GOT4.8 for short-period (< 1.2 cpd) -Self consistent equilibrium for: Node, Sa, Ssa -FES2012 for Mm, Mf and Mt	Ray, 1999
Non-tidal loadings	Atmospheric pressure: GEOS-FPIT numerical weather model (see Section 9.4.4.6 of the Appendix A) --- Continental water storage: GEOS-FPIT model, specifically TWLAND product (see Section 9.4.4.6 of the Appendix A) --- Ocean bottom pressure: OCMT model by the GFZ, specifically AOD1B product (see Section 9.4.4.6 of the Appendix A)	Rienecker et al., 2008 Reichle, 2011 Thomas, 2002 Dobslaw & Thomas, 2007
Glacial Isostatic Adjustment	For altimeter data correction: Global: ICE5G/Paulson or ICE6G AIS: IJ05_r2	Peltier, 2004 Paulson et al., 2007 Ivins et al., 2013

5.0 POD AND PPD CALIBRATION AND VALIDATION

5.1 Summary

As noted in Section 4.1, the POD team has the responsibility to calibrate and validate the parameters and products that comprise both POD and PPD deliverables. The product details are defined in the POD ICD. In this section we summarize the parameters and products to be calibrated and validated as well as the underlying methods and schedule. Table 5-1 provides the summary of the parameters and products to be calibrated and validated. The methods and approaches noted in Table 5-1 are referenced to the literature where appropriate.

The altimeter measurement models necessary for instrument pointing, ranging and timing parameter calibration are detailed in Appendix A Sections 9.4.3.1 – 9.4.3.4.

Table 5-1 POD and PPD Parameter and Product Calibration and Validation

Parameter/Product	Schedule	Method/Approach
POD Parameter Calibration		
Orbit prediction force model	Concentrated analysis during first 60 days with periodic reprocessing.	Tune parameters to minimize difference between 5-day orbit predicts and definitive orbits.
ICESat-2 radiative force panel model parameters		Tune parameters using GPS and independent SLR tracking data residual reduction and analysis, orbit comparisons, orbit overlap tests and independent direct altimetry and short-period altimeter crossover analysis. [Luthcke et al. 2003, Luthcke et al. 1997, Marshall and Luthcke 1994, Lemoine et al. 2010].
Reduced dynamic parameterization		
GPS antenna phase center offset vector and phase center variation map		
SLR Retro-Reflector optical center offset vector		
Center of Mass vector model parameters. Model is function of SA orientation and fuel depletion, and delivered to POD team from OSC.		
POD Product Validation and Error Estimate		
Precision Orbit in ICRF ANC02_p_yyyydddssss_vVV	Daily predict	5 day orbit predicts compared to definitive orbits. Tune error propagation.
Precision Orbit in ICRF ANC04_p_yyyydddssss_vVV	Daily orbit	GPS and independent SLR tracking data residual analysis, orbit comparisons, orbit overlap tests, and independent direct altimetry and short-period

Parameter/Product	Schedule	Method/Approach
		altimeter crossover analysis. [Luthcke et al. 2003,, Lemoine et al. 2010].
PPD Product Calibration		
Pointing vector in Laser Frame LF_PNTG_yyyydddsssss_vVV_cal.a	Daily Files	Calibrate components of pointing through reduction and analysis of direct altimetry from ocean scan maneuvers and short-period crossovers. Pointing biases, trends and orbital variation will be calibrated using the above noted data in 7-10 day batch solutions. As outlined below, time varying altimeter range-bias parameters are simultaneously estimated along with the pointing calibration parameters [Luthcke et al. 2000, Luthcke et al. 2002, Luthcke et al. 2005].
Laser Frame to Star Frame quaternions LF_2_SF_*yyyydddsssss*_v*VV*_cal.a		
Star Frame to J2000 Frame quaternions SF_2_J2000_*yyyydddsssss*_v*VV*.a		
Attitude timing bias	Beginning of mission and as needed	Reduction and analysis of direct altimetry from ocean scan maneuvers and short-period crossovers [Luthcke et al. 2000, Luthcke et al. 2002, Luthcke et al. 2005].
Altimeter Parameter Calibration		
Range timing bias	Beginning of mission and as needed	Reduction and analysis of direct altimetry from ocean scan maneuvers and short-period crossovers [Luthcke et al. 2000, Luthcke et al. 2002, Luthcke et al. 2005].
Time varying range bias for beams not monitored by the transmitter echo.	Concentrated analysis during first 60 days with 10-day updates continuing throughout mission.	Instrument team will deliver a model of time varying range bias as a function of temperature for all beams. On-orbit, the time-varying range bias for the beams observed by the transmitter echo will be used to tune the model of the un-observed beams using the telemetered temperatures. Then further tuning of the model parameters will be done from the reduction of short-period (< 24 hr.) cross-over data between observed and unobserved beams in 10-day batches. Solutions where the time varying range biases are estimated alone and in combination with the pointing parameter calibration will be compared.

5.2 Range Residual Analysis and Ocean Scan Maneuvers

Laser pointing, ranging, timing and orbit errors must be compensated in order to accurately geolocate the laser altimeter surface returns. The returned photon range observations can be

exploited in an integrated residual analysis to accurately calibrate these geolocation/instrument parameters [Luthcke et al. 2000, 2002, 2005]. For ICESat-2, as with ICESat-1, we apply this approach, processing ICESat altimeter range observations from ocean scans (OS) and "round"-the-world scans (RTWS) along with dynamic crossovers in order to calibrate and correct the systematic pointing and ranging errors (SP&RE) in the form of biases, trends and orbital variation parameters [Luthcke et al. 2005].

OS and RTWS are specifically designed calibrations that use commanded spacecraft attitude maneuvers and ocean altimeter range observations to recover pointing, ranging and timing parameters [Luthcke et al. 2000]. The parameters are estimated from a batch reduction of the altimeter range residuals using Bayesian least-squares differential corrections. The maneuver is a conic-like small amplitude (2 - 5°) deliberate roll and pitch deviation of the spacecraft attitude from nominal nadir pointing. Each 20 minute OS has two complete conic-like revolutions around the local nadir direction. The RTWS calibration maneuvers are simply OS maneuvers performed continuously over oceans for 1.5 orbit revolutions (performed for the tracks with the most ocean coverage). Detailed error analysis and application show these maneuvers are a strong filter for isolating systematic pointing errors from other systematic error sources such as ranging errors [Luthcke et al. 2000 and 2002]. Additionally, these calibrations are independent from the ice sheet data used in determining ice sheet surface elevation change.

For ICESat-1, the OS maneuvers are performed nominally twice per day over the mid-Pacific: one is done approximately at orbit noon and one approximately at orbit midnight to capture any instrument thermal-mechanical variation. Pointing biases in both the ATLAS Coordinate System (ACS) X and Y axes, along with a range bias, are estimated through the reduction of the ocean surface altimeter range residuals from each OS. The RTWS calibrations are performed nominally every 8-days during the orbit track that has the most ocean coverage, and provide a means to estimate remaining SPE orbital variation as a function of orbit angle (angle between the satellite position vector and the sun vector projected in the orbit plane where 0° is orbit 6AM and 90° is orbit noon). Through the reduction of the range residuals from the RTWS, pointing biases in both the ACS X and Y axes are nominally estimated every 7.7 minutes or every 30° in orbit angle. The resulting OS and RTWS calibration history facilitate sub-arcsecond calibration of SPE (orientation and amplitude) at time scales of ~8-minutes to months [Luthcke et al. 2002, 2005].

The altimeter measurement models necessary for instrument pointing, ranging and timing parameter calibration are detailed in Appendix A Sections 9.4.3.1 – 9.4.3.4. The algorithms were implemented into NASA/GSFC's GEODYN precise orbit and geodetic parameter estimation software in order to take advantage of the existing robust estimation scheme and the myriad of model parameters, as well as to leverage combining the altimeter data with other tracking data types. The estimation process is documented in Section 9.1 of Appendix A. GEODYN has a strong set of Multi Beam Laser Altimeter (MBLA) data processing capabilities. Furthermore, GEODYN can process individual laser altimeter range observations as a tracking data type (direct altimetry). It is also possible to pair altimeter observations, which are taken at the same

Earth fixed location (but at different times), into a distinct tracking data type called crossovers. Each of these applications of altimetry is described in the Appendix. GEODYN can also simultaneously process and estimate parameters associated with each of the lasers individually in the MBLA instrument.

6.0 TEST DATA AND RESULTS

6.1 Unit Test Data

6.1.1 Unit Test 1 Purpose

Repeat for as many unit tests as needed to test each condition in the algorithm. What functions of the algorithm it will test and algorithm expectation.

6.1.1.1 Unit Test Inputs

Specific value(s) for each input or sets of values to allow simple unit testing that validates the algorithm is implemented as specified.

6.1.1.2 Results

The resulting value(s) for each output parameter based on the inputs

6.2 Simulated Test Data

Repeat as many simulation data sets as needed to test each condition in the algorithm.

6.3 Simulated Data Set 1

6.3.1.1 Source

Description of the data set, what functions of the algorithm it will test and algorithm expectation. Name and source location of the data set

Repeat for as many as simulation tests as needed.

6.3.1.2 Results

Description of the results from the data set being processed by the algorithm. Name and source location of the expected resulting values from processing the data set.

7.0 CONSTRAINTS, LIMITATIONS, AND ASSUMPTIONS

TBD- as needed.

8.0 GLOSSARY/ACRONYMS

ACS	ATLAS Coordinate System IN
ASAS	ATLAS Science Algorithm Software
ATLAS	ATLAS Advance Topographic Laser Altimeter System
ATBD	Algorithm Theoretical Basis Document
C/A	civilian access code
CDDIS	Crustal Dynamics Data Information System, GSFC
CLS	Collecte Localisation Satellites, France
CoM	center of mass
GSFC	Goddard Space Flight Center
GNSS	Global Navigation Satellite Systems
ICD	Interface Control Document
ICESat-2	ICE, CLOUD, and Land Elevation Satellite
ICESat-2 MIS	ICESat-2 Management Information System
ICRF	International Celestial Reference Frame
IGS	International GNSS Service
ITRF	International Terrestrial Reference Frame
ITRF-FR	International Terrestrial Reference Frame Service, France
IERS	International Earth Rotation Service
JD	Julian Date
JPL	Jet Propulsion Laboratory, IGS Central Bureau
MBLA	Multi-Beam Laser Altimeter
MJD	Modified Julian Date
MOC	Mission Operations Center
MSIS	Mass Spectrometer – Incoherent Scatter
NGA	National Geospatial Intelligence Agency
NOAA	National Oceanic and Atmospheric Administration
OS	ocean scans
PAN	product acceptance notice

PDR	product delivery notice
PGS	Precision Geolocation System
PPD	Precision Pointing Determination
PPN	parameterized post-Newtonian
POD	Precision Orbit Determination
PSO	ICESat-2 Project Support Office
RGT	Reference Ground Track
RTWS	“round”-the-world scans
SCoRe	Signature Controlled Request
SDMS	Scheduling and Data Management System
SIPS	Science Investigator-Lead Processing System
SP&RE	systematic pointing and ranging errors
TAI	International Atomic Time
TOD	True of Date
TOR	True of Reference
TDT	Terrestrial Dynamic Time
TT	Terrestrial Time
USGS	U.S. Geological Survey
USNO	United States Naval Observatory

9.0 APPENDIX A ALGORITHMS AND METHODS DETAILS

9.1 Parameter Estimation

The purpose of this section is to provide a general understanding of the methods used in the solution of the parameter estimation problem. The following overview is a summarized direct excerpt from the GEODYN documentation [*Pavlis et. Al., 1998*].

Consider the relationships between the observations, O_i, their corresponding computed values, C_i, and the vector of parameters to be determined, P. These relationships are given by:

$$O_i - C_i = -\sum_j \frac{\partial C_i}{\partial P_j} dP_j + dO_i \qquad (9.1.1)$$

where

i denotes the i^{th} observation

dP_j is the correction to the j^{th} parameter

dO_i is the error of observation associated with the i^{th} observation

The basic problem of parameter estimation is to determine a solution to these equations.

The role of data preprocessing is made apparent from these equations. First, the observation and its computed equivalent must be in a common time and spatial reference system. Second, there are certain physical effects such as atmospheric refraction, which do not significantly vary with any likely change in the parameters represented by the vector P, allowing these types of computations and corrections to be applied to either the observations or to their computed values. The relationship between the computed value and the model parameters, P, is in general nonlinear, and thus the estimation process will not converge in a single iteration, requiring that the computed values be evaluated repeatedly in several iterations of the estimation procedure. Thus a considerable increase in computational efficiency may be attained by applying these computations and corrections to the observations; *i.e.*, to preprocess the data.

The preprocessed observations used by GEODYN are directly related to the position and/or velocity of the satellite relative to the observer or altimeter bounce point at the given observation time. These relationships are geometric; hence computed observations are obtained from the geometric relationships of the positions and velocities of the satellite and the observer or bounce point at the desired time (the measurement model).

Associated with each measurement is a (known) statistical uncertainty. This uncertainty is a statistical property of the noise on the observations. In addition, there are generally more observations than parameters, and thus the parameters are over-determined. Therefore, a statistical estimation procedure is required for the parameter determination.

It should be noted that dO_i, the observation error, is not the same as the noise on the observations. The dO_i account for all of the discrepancy, $O_i - C_i$, which is not accounted for by the corrections to the parameters, dP, and therefore represent both the contribution from the noise on the observation, and the incompleteness of the mathematical model represented by the parameters, P. By this last expression, we mean either that the estimated parameter set is insufficient to model the physical situation, or that the functional form of the model is inadequate. GEODYN has two different ways of dealing with these observation errors: (1) the measurement model includes measurement and timing bias parameters to be estimated and (2) there is an automatic editing procedure to delete bad (*i.e.* statistically unlikely) observations.

The nature of the parameters to be determined has a significant effect on the functional structure of the solution. In GEODYN, these parameters are:

- *Satellite position and velocity at epoch*. These are the initial conditions for the equations of motion.
- *Force model parameters*. These define the motion of the satellite.
- *Measurement model parameters*. These include the geophysical and bias parameters and do not affect the motion of the satellite.

Thus, the parameters to be determined, P, are implicitly partitioned into a set $\bar{\beta}$, which are concerned with the dynamics of the satellite motion, and a set $\bar{\alpha}$, which are not.

The computed value, C_i, for each observation, O_i, is a function of the position vector of the observer, $\bar{r}_{ob}$, and the true of date position and velocity vector of the satellite at the desired observation time, $\bar{x}_t$. When measurement biases are used, C_i is also a function of $\bar{B}$, the biases associated with the particular measurement type. Let us consider the affect of the given partitioning on the required partial derivatives in the observational equations:

$$\frac{\partial C_i}{\partial P_j} \quad \Rightarrow \quad \frac{\partial C_i}{\partial \bar{\alpha}} = \left[\frac{\partial C_i}{\partial \bar{r}_{ob}}, \frac{\partial C_i}{\partial \bar{B}} \right], \quad \frac{\partial C_i}{\partial \bar{\beta}} = \frac{\partial C_i}{\partial \bar{x}_t} \frac{\partial \bar{x}_t}{\partial \bar{\beta}} \qquad (9.1.2)$$

where

$\frac{\partial \bar{x}_t}{\partial \bar{\beta}}$ are the variational partial derivatives

The partial derivatives of the computed value with respect to $\bar{r}_{ob}$, $\bar{B}$, and $\bar{x}_t$, are determined from the measurement model at the given time. In order to compute the variational partials it is necessary to numerically integrate the "variational equation," which is a similar process to the integration of the equations of motion that is performed to compute the orbit.

The elements of the observational equations have been discussed above; the following discusses the solution of these equations; *i.e.*, the statistical estimation scheme. There are a number of

estimation schemes that can be used. The method used in GEODYN is a batch scheme that uses all observations simultaneously to estimate the parameter set. The alternative would be a sequential scheme that uses the observations sequentially to calculate an updated set of parameters from each additional observation. Although batch and sequential schemes are essentially equivalent, practical numerical problems often occur with sequential schemes, especially when processing highly accurate observations and estimating large parameter sets.

The particular method selected for GEODYN is a partitioned Bayesian least squares method. A Bayesian method in particular is used due to the utilization of meaningful *a priori* information. The Bayesian estimation formula is given as:

$$d\vec{x}^{(n+1)} = \left[B^T W B + V_A^{-1}\right]^{-1}\left[B^T W d\vec{m} + V_A^{-1}\left[\vec{x}_A - \hat{\vec{x}}^{(n)}\right]\right] \qquad (9.1.3)$$

where,

$\vec{x}_A$	is the *a priori* estimate of the vector of parameters
V_A	is the *a priori* covariance matrix associated with the a priori estimate of the parameters
W	is the weighting matrix associated with the observations
$\vec{x}^{(n)}$	is the n^{th} approximation of the true solution of the parameters
$d\vec{m}$	is the vector of residuals from the n^{th} approximation
B	is the matrix of partial derivatives of the measurements with respect to the parameters, number of measurements by number of parameters
$d\vec{x}^{(n+1)}$	is the vector of corrections to the parameters, *i.e.*, $\vec{x}^{(n+1)} = \vec{x}^{(n)} + d\vec{x}^{(n+1)}$

Since GEODYN has multi-arc multi-satellite capabilities, the estimation scheme is efficiently implemented such that all arcs are not needed in memory simultaneously. This partitioning separates all the parameters into two categories: arc parameters, which are associated with separate time periods, and global parameters, which are common to all arcs in the data reduction or orbit generation run. This partitioning dramatically reduces the memory requirements of the program without any significant cost in computation time.

9.2 Reduced Dynamic Technique

There are several GPS-based POD strategies that can be utilized to determine the orbit of a satellite. The kinematic approach takes advantage of the fact that GPS measurements provide multiple simultaneous observations that allow instantaneous geometrical solutions for the satellite position. Such an approach, however, de-couples the orbit determination problem from

that of the force and measurement model improvement, and it does not take advantage of any information provided from the underlying orbital dynamics.

Alternatively, the dynamic technique uses the GPS data to estimate updates to the parameters that define the dynamical motion of the satellite, thus refining the orbit in the process. This approach generally only estimates a few parameters which are directly related to uncertainties in the physical models, and which affect the satellite over the entire arc, or over relatively long periods of time.

The reduced dynamic technique is commonly regarded as the optimal GPS-based orbit determination strategy, as it is an intermediate approach that includes both the orbit dynamics and the geometric strength of instantaneous solutions. This method involves solving for a large number of empirical parameters, which are usually acceleration parameters that describe the difference between the actual acceleration that a satellite experiences, and the acceleration that is predicted by the physical models of the orbit determination program.

Though the reduced dynamic approach has proven successful for a number of satellite missions, it must be recognized that the reduced dynamic process begins with a dynamic orbit solution that already has attained sufficient radial accuracy. Even though reduced dynamic approaches are employed to overcome the inadequacies of physical models, it has been shown that the technique relies on good physical models, and improvements in the orbit fit are realized when the models are improved. In other words, dense tracking and the reduced dynamic technique do not obviate the use of accurate orbit modeling.

The use of large numbers of empirical parameters requires either the presence of dense tracking with sufficient geometric strength, or the use of some type of constraint information during the estimation process, or possibly both. For example, Kalman filtering techniques, on the strength of covariance functions, can allow the time period of an adjusted parameter to be as small as the interval between observations. Constraint equations can be developed to give some of the advantages of Kalman filtering while still using a standard batch least square estimator.

GEODYN uses a standard Bayesian least squares estimator, and thus, in addition to standard observation equations, constraint equations can be used to force adjusted parameters to stay “close” to *a priori* values. In practice, the GEODYN user supplies an *a priori* parameter value and an *a priori* parameter standard deviation for each adjusted parameter. The weight of an *a priori* value constraint equation is the reciprocal of the square of the standard deviation. The *a priori* constraint equations are the only type of constraint equations available in a standard version of GEODYN. A limitation of this type of constraint equation is that as the number of adjusted parameters is increased, the weight on each *a priori* constraint equation must also be increased, meaning that the more empirical parameters that are estimated, the more tightly each must be held to some initial value. In the case of empirical accelerations, the initial value is usually zero, so as more parameters are adjusted, the increase in frequency information comes at the expense of limiting the magnitude of these accelerations to an increasingly tight envelope around zero.

The *a priori* constraint weights can be loosened a bit if a second class of constraint equations is added which force continuity between similar parameters by constraining all empirical parameters of the same type to be equal to one another. Constraint equations linking parameters from adjacent time periods are given much larger weights than constraint equations linking time periods that are separated by a large interval of time. That is accomplished by the specification of an "adjacent" weight (W_o) and an exponential decay factor (Δ). The weight given to the constraint equation to tie period number *i* to period number *j* is:

$$W = W_0 e^{-\Delta|i-j|} \quad (9.2.1)$$

These continuity constraints are useful in finding a balance between the number of estimated parameters, the level of fit to the tracking data, and the orbit overlap consistency.

9.3 Orbit Modeling

9.3.1 Equations of Motion

Orbit prediction in GEODYN utilizes Cowell's method, which is the direct numerical integration of the satellite equations of motion in inertial rectangular coordinates. The equation of motion for an Earth-orbiting satellite may be described as:

$$\ddot{\vec{r}} = \vec{a}_c + \vec{a}_{nc} + \vec{a}_{emp} \qquad (9.3.1.1)$$

where

$\ddot{\vec{r}}$ = satellite acceleration

$\vec{a}_c$ = sum of all conservative forces

$\vec{a}_{nc}$ = sum of all non-conservative forces

$\vec{a}_{emp}$ = sum of all empirical accelerations

The initial conditions for these differential equations are the epoch position and velocity, and the accelerations of the satellite at each epoch must be evaluated from the force model. The equations of motion for the satellite must be integrated in an inertial coordinate system. The GEODYN inertial system is the True of Reference system (TOR), which is defined as the True of Date (TOD) system corresponding to some reference epoch. The coordinate systems in which the accelerations due to each physical effect are evaluated vary. The geopotential accelerations are evaluated in the Earth-fixed system, and then transformed to the inertial system to be combined with the other accelerations, which are evaluated in the TOD inertial system. The total acceleration is then transformed to the TOR inertial system for use in the integration procedure.

The integration procedure used in GEODYN is a Cowell predictor-corrector type with a fixed order and a fixed time step. The integration algorithms used output satellite position and velocity on an even time step, so an interpolation procedure is required for positions and velocities at other times.

9.3.2 Time Systems

The integration of the satellite equations of motion requires a uniform time system. The system used in GEODYN is the Terrestrial Dynamic Time (TDT) (also referred to as Terrestrial Time (TT)) [*Guinot, 1991, McCarthy, 1996*]. The TDT time is in practice determined from the International Atomic Time (TAI):

$$TDT = TAI + 32.184 \text{ s} \qquad (9.3.2.1)$$

The TDT time must be converted to the conventional time scales used by most observers for time-tagging satellite observations and tracking data. The conventional time scales relevant to most laser altimeter missions are UTC and GPS time.

UTC, or Coordinated Universal Time, is an atomic time system which runs at the same rate as TAI, but is periodically adjusted by one second steps in order to keep it near the UT1 time system. The UT1 time system is the non-uniform time determined by observations of the stars from the non-uniformly rotating Earth, after correcting for polar motion. Correction factors relating UTC and UT1, and UTC and TAI, are provided by the IERS Bulletin B or by the USNO Rapid Service (IERS Bulletin A).

GPS Time [*Hofmann-Wellenhof et al., 1994*] is the time system to which all GPS clocks and observables are referenced. It is also an atomic time system derived from TAI. GPS Time can be computed from:

$$GPS = TAI - 19.000 \text{ s} \qquad (9.3.2.2)$$

Calendar dates are referenced to the Julian Date (JD) or the Modified Julian Date (MJD) [*Taff, 1985*]. The current standard epoch is J2000.0 which is JD = 2451545.0, or January 1.5, 2000.

The GPS system uses the GPS standard epoch of JD = 2444244.5 or January 6.0, 1980. An important unit for the GPS system is the GPS week, which is defined as:

$$\text{GPS week} = \text{INT}\,[(JD - 2444244.5) / 7] \qquad (9.3.2.3)$$

where INT[x] is the largest integer smaller than x.

9.3.3 Reference Frames

The current ECI frame employed for the ICESat-2 altimeter measurement modeling and geolocation is the geocentric realization of the International Celestial Reference System (ICRS), namely the ICRF Geocentric mean equator and equinox of 2000 Jan 1.5 (J2000.0) defined by the International Earth Rotation Service (IERS), and realized by use of the JPL Development Ephemeris DE403, and the Lunar Ephemeris LE403 [Standish et al., 1995 & *Petit and Luzum, 2010*].

The geodetic reference frame, which is consistently used in the analysis of altimeter data, is the International Terrestrial Reference Frame (ITRF). The ITRF definition and other current modeling recommendations of the IERS are documented in the "IERS Conventions" [*Petit and Luzum, 2010*].

Transformation between the ICRF and the ITRF is accomplished using the following equation:

$$\left[ICRF\right] = P(t)N(t)R(t)W(t)\left[ITRF\right] \quad (9.3.3.1)$$

where

P(t) = precession transformation
N(t) = nutation transformation
R(t) = transformation due to rotation of the Earth
W(t) = polar motion transformation

The precession – nutation transformations follows IAU 2000 [*Cappola et al., 2009*]. The rotation transformation is just a rotation around the Earth's spin axis by $-\theta_g$, where θ_g is the Greenwich True Sidereal Time at epoch *t*. The *R(t)* and *W(t)* transformations are described in [*Petit and Luzum, 2010*].

9.3.4 Conservative Force Modeling

This section summarizes the modeling of the conservative forces, which are gravitational in nature and can be derived from a potential. The satellite acceleration due to the conservative forces can be described by:

$$\vec{a}_c = \vec{a}_{geo} + \vec{a}_{tides} + \vec{a}_{dyn} + \vec{a}_{tvg} + \vec{a}_{n-body} + \vec{a}_{rel} \quad (9.3.4.1)$$

where

$\vec{a}_{geo}$ is the acceleration due to the static geopotential

$\vec{a}_{tides}$ is the acceleration due to solid Earth and ocean tides

$\vec{a}_{dyn}$ is the effect of dynamic polar motion

$\vec{a}_{tvg}$ is the acceleration from time variable gravity

$\vec{a}_{n-body}$ is the result of N-body perturbations, primarily the Sun and Moon

$\vec{a}_{rel}$ is the contribution from general relativity

These various components of the conservative forces are now discussed.

9.3.4.1 Geopotential

The geopotential represents the static gravity field and describes the large majority of mass in the Earth system. The acceleration due to the geopotential is described by:

$$\vec{a}_{geo} = \nabla U \qquad (9.3.4.1.1)$$

where

$$U = \frac{GM}{r}\left[1 + \sum_{n=2}^{n\max}\sum_{m=0}^{n}\left[\frac{a_e}{r}\right]^n P_n^m(\sin\phi)\left[C_{nm}\cos m\lambda + S_{nm}\sin m\lambda\right]\right] \qquad (9.3.4.1.2)$$

G is the universal gravitational constant

M is the mass of the Earth

r is the geocentric satellite distance

n max is the highest degree of the field

a_e is the Earth's mean equatorial radius

ϕ is the satellite geocentric latitude

λ is the satellite east longitude

$P_n^m(\sin\phi)$ are the associated Legendre functions

C_{nm}, S_{nm} are the denormalized gravitational coefficients

The geopotential model to be used is GIF48 [*Ries et al., 2011*]. This model, complete to degree and order 360, was determined with a combination of 66 months of GRACE data and terrestrial information taken from the DT10 global gravity field [*Anderson, 2010*], and is considered to be the current state-of-the-art.

9.3.4.2 Solid Earth Tides and Ocean Tides

The largest component of the time variations in the conservative forces is the solid Earth and ocean tides, which are caused by the effect that the gravitational attraction of the Sun, Moon, and planets have in redistributing the solid Earth and liquid water mass of the Earth. This time-dependent redistribution of Earth mass from equilibrium alters the gravitational field of the Earth, thus perturbing the motion of orbiting satellites.

*****This section needs to be completed.**

9.3.4.3 Dynamic Polar Motion

Variations in the rotation of the Earth produce changes in the centrifugal force throughout the Earth. These changes produce a time-varying deformation of the Earth, which may be expressed by introducing a time-dependence in the C_{21} and S_{21} geopotential coefficients [*Lambeck, 1980, and McCarthy, 1996*].

GEODYN models these changes by: (1) rotating the coordinate system for evaluation of the geopotential to make the *Z*-axis coincident with the instantaneous axis of the Earth's rotation, including the effect of polar motion ("GEOPOL" option), and by (2) modifying the C_{21} and S_{21} coefficients to account for the gravitational effects of the deformation of the earth due to polar motion. The modified C_{21} and S_{21} coefficients are:

$$C_{21}(t) = \hat{C}_{21} + \sqrt{3} K_f \hat{C}_{20} \left[x_p(t) - \left(\bar{x}_p(t_0) + \dot{\bar{x}}_p \cdot (t - t_0) \right) \right]$$
$$S_{21}(t) = \hat{S}_{21} - \sqrt{3} K_f \hat{C}_{20} \left[y_p(t) - \left(\bar{y}_p(t_0) + \dot{\bar{y}}_p \cdot (t - t_0) \right) \right] \qquad (9.3.4.3.1)$$

where

t_0	is the epoch of the six year average of the polar motion axis
$x_p(t), y_p(t)$	are pole values at time t
$\bar{x}_p(t_0), \bar{y}_p(t_0)$	are the pole values corresponding to the six year average of the polar motion axis
$\dot{\bar{x}}_p(t_0), \dot{\bar{y}}_p(t_0)$	are drift rates for the six year average pole values
$\hat{C}_{20}, \hat{S}_{21}, \hat{C}_{21}$	are the normalized geopotential coefficients referenced to the Conventional Terrestrial Reference System

and K_f is the figure axis scale factor, which is equal to the ratio k_2/k_s, where k_2 is the Earth's Love number (≈ 0.30) and k_s is the "secular Love number" (≈ 0.94) [*Gross, 1994*]. The modification of the C_{21} and S_{21} coefficients is controlled by the option "POLDYN", and the value of K_f may be set using the option "POLKF".

9.3.4.4 Time Dependent Gravity

The GEODYN program allows time variations in the geopotential coefficients so that they can be expressed as:

$$\begin{aligned} C_{nm}(t) &= C_{nm}(t_0) + A_{Cnm}\cos\left(\omega(t-t_0)\right) + B_{Cnm}\sin\left(\omega(t-t_0)\right) + \dot{C}_{nm}(t_0)\cdot(t-t_0) \\ S_{nm}(t) &= S_{nm}(t_0) + A_{Snm}\cos\left(\omega(t-t_0)\right) + B_{Snm}\sin\left(\omega(t-t_0)\right) + \dot{S}_{nm}(t_0)\cdot(t-t_0) \end{aligned} \qquad (9.3.4.4.1)$$

where

t	is the current time
t_0	is the reference epoch for the static coefficient
A, B	are the coefficients of the cosine and sine terms, respectively
ω	is the frequency of the sinusoidal variation
$\dot{C}_{nm}(t_0), \dot{S}_{nm}(t_0)$	is the linear rate in the coefficient at time t_0

This capability is controlled by the option "GRVTIM".

9.3.4.5 N-body Perturbations

N-body perturbations refer to the forces exerted on the satellite by bodies other than the Earth. GEODYN can apply N-body perturbations due to the Sun, Moon and all the planets. It uses the following formulation of the perturbing acceleration:

$$\vec{a}_{n-body} = -Gm_d\left[\frac{\vec{d}}{D_d} + \frac{\vec{r}_d}{r_d}\right] \qquad (9.3.4.5.1)$$

where

$$\vec{d} = \vec{r} - \vec{r}_d$$

$$D_d = \left[r_d^2 - 2rr_dS + r^2\right]^{\frac{3}{2}}$$

m_d is the mass of the disturbing body

$\vec{r}_d$ is the geocentric true of date position vector to the disturbing body

S is the cosine of the enclosed angle between r_d and r.

$\vec{r}$ is the geocentric true of date position vector of the satellite

G is the universal gravitational constant

The geocentric positions of the Sun, Moon and the planets are derived from the input planetary ephemerides, currently the DE403 and LE403 [*Standish et al., 1995*].

9.3.4.6 Relativistic Force Models

The exact solution to the problem of a satellite orbiting a massive body is difficult to obtain in general relativity theory. For Earth satellites, the masses and velocities involved are small, so the "post-Newtonian" approximation is made. In this approximation, the satellite motion is Newtonian, although perturbed by small additional forces which represent the effects of the general relativity. The total relativistic perturbation is described by three terms that are developed below:

$$\vec{a}_{rel} = \vec{a}_{pm} + \vec{a}_{gp} + \vec{a}_{LT} \qquad (9.3.4.6.1)$$

The first "post-Newtonian" effect is the modification of the point-mass central body acceleration. Following *Soffel* [*1989*], this additional acceleration is:

$$\vec{a}_{pm} = \frac{GM_E}{c^2}\left[\frac{4GM_E}{r^4}\vec{r} - \frac{\vec{v}^2}{r^3}\vec{r} + 4\frac{(\vec{r}\cdot\vec{v})}{r^3}\vec{v}\right] \qquad (9.3.4.6.2)$$

where

$\vec{r}, \vec{v}$ are the inertial planet-centered position and velocity of the spacecraft

M_E is the mass of the Earth

G is the universal gravitational constant

and the parameterized post-Newtonian (PPN) parameters β and γ have both been set equal to one, their values in Einstein's general relativity.

The next additional relativistic acceleration is due to geodetic precession (also known as the relativistic Coriolis force) [*Huang et al., 1990*]. This acceleration is due to the precession of the axis of a freely falling inertial frame. Thus, the inertial planet-centered frame precesses with respect to the inertial barycentric frame with angular velocity (if the sun is considered the only contributor) is given by:

$$\vec{\Omega} = \frac{3}{2}\left(\vec{V}_E - \vec{V}_S\right) \times \left[\frac{-GM_S \vec{X}_{ES}}{c^2 R_{ES}^3}\right] \qquad (9.3.4.6.3)$$

where

$\vec{X}_E, \vec{V}_E$ are the barycentric position and velocity of the central body

$\vec{X}_S, \vec{V}_S$ are the barycentric position and velocity of the sun

$\vec{X}_{ES} = \vec{X}_E - \vec{X}_S$

$R_{ES} = \left|\vec{X}_E - \vec{X}_S\right|$

M_S is the mass of the sun

This precession exhibits itself as an acceleration on a spacecraft orbiting the central body much like the Coriolis force. Therefore, the contribution to the equations of motion implemented in GEODYN is given by:

$$\vec{a}_{gp} = 2\left(\vec{\Omega} \times \vec{v}\right) \qquad (9.3.4.6.4)$$

where $\vec{v}$ is the inertial planet-centered velocity of the spacecraft.

The third additional relativistic effect is the Lense-Thirring acceleration. This is due to the mass current and gravito-magnetic field of a rotating gravitating body. A very simple explanation for this is given in *Soffel, 1989*; "A rotating central body influences the surrounding space-time in some sense similar as if it were immersed in a viscous fluid transferring some of its rotational energy to the surrounding medium." The effect on an orbiting spacecraft is to drag the angular momentum vector of the orbit along with the rotating central body. The contribution to the equations of motion [*Huang et al., 1990*] is implemented in GEODYN as:

$$\vec{a}_{LT} = 2\frac{GM_E}{c^2 r^3}\left[\frac{3}{r^2}\left(\vec{r} \times \vec{v}\right)\left(\vec{r} \cdot \vec{J}\right) + \left(\vec{v} \times \vec{J}\right)\right] \qquad (9.3.4.6.5)$$

where

$\vec{r}, \vec{v}$ are the inertial planet-centered position and velocity of the spacecraft

G is the universal gravitational constant

$\vec{J}$ is the angular momentum of the Earth per unit mass, $\left|\vec{J}\right| \cong 9.8 \times 10^8$ m^2 / sec

M_E is the mass of the Earth

9.3.5 Non-Conservative Force Modeling

The following sections briefly discuss the modeling of the non-conservative forces, which dissipate the energy of a satellite and can be describe by:

$$\vec{a}_{nc} = \vec{a}_{drag} + \vec{a}_{solar} + \vec{a}_{Earth} + \vec{a}_{thermal} \qquad (9.3.5.1)$$

where

$\vec{a}_{drag}$ is the acceleration due to atmospheric drag

$\vec{a}_{solar}$ is the acceleration due to solar radiation pressure

$\vec{a}_{Earth}$ is the acceleration due to Earth radiation pressure

$\vec{a}_{thermal}$ is the acceleration caused by thermal imbalance

In order to achieve the orbit accuracy required for ICESat-2, it is critical that the non-conservative forces be well modeled. To do this effectively requires that the size, shape, and material characteristics of the spacecraft surfaces that interact with these forces be well modeled. This is achieved in GEODYN by modeling the spacecraft as a series of flat plates oriented in space, where each plate possesses its own properties, which are determined by the aggregate composition of the spacecraft material properties represented by that particular macro-model plate. These material properties include the area, specular reflectivity, diffuse reflectivity, emissivity, and in some cases temperature parameters [*Luthcke, 1992*]. The non-conservative forces acting on each flat plate are then computed independently and summed to calculate the overall acceleration on the spacecraft center of mass:

$$\vec{a}_{nc\ total} = \sum_i \vec{a}_{nc\ i} \qquad (9.3.5.2)$$

where *i* represents each individual flat plate in the full macro-model, and the set of non-conservative forces developed below describe the perturbing effect on a single plate.

Precise modeling of the spacecraft accelerations with macro-models as described above depends on knowledge of the spacecraft attitude. GEODYN has the ability to model the nominal orientation of the spacecraft with time, and this approach can be used in cases where attitude data is unavailable. Otherwise the estimated orbits will make use of either the onboard attitude solution (rapid POD) or the rapid PAD product (final POD) to provide GEODYN with a time history of ICESat-2 quaternions.

9.3.5.1 Atmospheric Drag

Near-Earth satellites travel through a rarefied atmospheric medium. The acceleration of a spacecraft caused by its interaction with the Earth's atmosphere can be described by:

$$\vec{a}_{drag} = -\frac{1}{2} C_D \frac{A}{m} \rho(x,t)\, V_r \vec{V}_r \qquad (9.3.5.1.1)$$

where

C_D	is the satellite drag coefficient
A	is the satellite cross-sectional area projected normal to the v
m	is the satellite mass
$\rho(x,t)$	is the atmospheric density at position x and time t
$\vec{V}_r$	is the satellite velocity relative to the atmosphere

The atmospheric density to be applied in GEODYN is the MSIS (Mass Spectrometer – Incoherent Scatter) model, which is based on *in situ* atmospheric spectrometer measurements [*Hedin, 1987*]. This model, and others that are in general use, suffer from incomplete global coverage, long time constants requiring considerable averaging, and extrapolations for altitudes higher than 800 km. The current density models are largely inadequate to produce atmospheric density profiles that suitably support precision orbit determination requirements. It is thereby a common practice to use the strength of the satellite tracking data and adjust drag-scaling parameters to enhance the accuracy of the results.

9.3.5.2 Solar Radiation Pressure

There are three sources of radiative forces which act on a satellite: (1) the solar radiation force which is due to the pressure of direct sunlight on the spacecraft, (2) the Earth re-radiation force which is due to the pressure of Earth-reflected sunlight and Earth thermal emission, and (3) thermal imbalance forces, which result from a net flux of thermal radiation from the spacecraft body. The satellite accelerations from each of these forces is given below.

Modeling of the direct solar radiation force on a spacecraft requires: (1) modeling the radiative flux from the Sun; (2) determining the geometry and orientation of the illuminated surfaces; and (3) modeling the interaction between these surfaces and the solar flux.

The magnitude of solar flux is well known. The distance from the satellite to the sun, and the direction of the satellite-sun vector must be computed, and any shadowing by the Earth or a third-body must also be considered.

The acceleration of the spacecraft due to solar radiation incident on one body plate is [*Nerem et al., 1993*]:

$$\vec{a}_{solar} = -\sum_i \frac{GA_i \cos\theta_i}{Mc}\left[2\left(\frac{\delta_i}{3} + \rho_i \cos\theta_i\right)\hat{n} + \left(1-\rho_i\right)\hat{s}\right] \qquad (9.3.5.2.1)$$

Where

A_i is the surface area of the flat plate

θ_i is the angle between the surface normal and source vectors

G is the radiation flux from the source

$\hat{n}$ is the surface normal unit vector

$\hat{s}$ is the source incidence unit vector

ρ_i is the specular reflectivity (percentage of total incoming radiation)

δ_i is the diffusive reflectivity (percentage of total incoming radiation)

M is the satellite mass

c is the speed of light

9.3.5.3 Earth Radiation Pressure

The spacecraft experiences additional acceleration from the pressure of solar radiation reflected by the Earth (albedo), and also from the thermal (infrared) radiation of the Earth [*McCarthy and Martin, 1977, Knocke et al., 1988*]. GEODYN models this radiation with a grid of latitude-longitude blocks, each of which has a specified optical reflectivity and infrared emissivity. GEODYN employs a computationally efficient method following *McCarthy and Martin* [*1977*] computing the acceleration on a surface as:

$$\vec{a}_{Earth} = -\sum_i^N \sum_j^{19} \frac{G_j A_i \cos\theta_{ij}}{Mc}\left[2\left(\frac{\delta_i}{3} + \rho_i \cos\theta_{ij}\right)\hat{n}_i + \left(1-\rho_i\right)\hat{s}_j\right] \qquad (9.3.5.3.1)$$

where j is the Earth spot of interest, and the sum over i represents the set of macro-model plates, and the other terms are the same as defined in the previous section.

9.3.5.4 Thermal Imbalance

Spacecraft are heated by the power dissipated from their internal components, and by incident external radiation from direct sunlight, Earth-reflected sunlight and infrared radiation from the Earth. The spacecraft re-radiates thermal radiation, and, if this radiation is not uniform in all directions, there will be a recoil acceleration of the spacecraft caused by the net momentum carried by the thermal radiation.

If the radiation follows a Lambertian distribution, the force exerted on each plate of the macro-model is [*Nerem et al., 1993*]:

$$\vec{a}_{thermal} = -\frac{2A\sigma}{3c}\varepsilon T^4 \hat{n} \qquad (9.3.5.4.1)$$

where

ε is the emissivity

σ is the Stefan-Boltzmann constant (5.67×10^{-8} W m^{-2}K^{-4})

A is the surface area (m^2)

T is the temperature (°K)

c is the speed of light (m/s)

$\hat{n}$ is the surface normal unit vector

The dependence of this expression on the plate temperature requires modeling of the time history of the plate temperature. The temperature as a function of time depends on various factors, such as material composition of the plate, orientation with respect to external radiation sources, thermal characteristics of the surface coating, etc., and must be modeled in a manner unique to each spacecraft. *Nerem et al.* [*1993*] contains a thorough discussion of how this temperature history was modeled for TOPEX/Poseidon. A similar model specific to ICESat-2 would need to be constructed if the mismodeling of this force was deemed to be a significant effect.

9.3.5.5 ICESat-2 Macro-model

Information regarding the ICESat-2 macro-model will be placed here once it becomes available. The pre-launch values describing the material properties given here will likely be refined as a part of the POD process.

9.3.6 Empirical Accelerations

The high fidelity force models implemented within GEODYN are quite robust and represent the state-of-the-art in spacecraft force modeling for efficient POD. However, there still remain force model errors that result in residual accelerations. Most of these are due to deficiencies in the models, such as poor modeling of temporal variations in atmospheric density, or are the result of model parameters not matching reality. For example, the best available attitude information may not be correct or good enough for the required level of modeling, or the pre-launch reflectivity of a satellite surface might not be the same as the reflectivity several months or years after launch, owing to deterioration of the surface coating.

To account for unknown residual accelerations, GEODYN has the capability to apply and solve for a set of generic spacecraft accelerations. These equations have the form:

$$\vec{a} = \left(A\cos(\omega t) + B\sin(\omega t) + C\right)\ \hat{u} \qquad (9.3.6.1)$$

where

$\vec{a}$	is the computed empirical acceleration
A, B, C	the adjustable parameters
ω	is the orbital frequency of the satellite
$\hat{u}$	is the unit vector in the selected direction

The GEODYN program allows accelerations to be applied in various coordinate systems, the most common being the HCL system (*i.e.* radial, cross-track and along-track). Several accelerations may be simultaneously applied and they may be defined to be independent in selected time periods.

9.4 Measurement Modeling

9.4.1 SLR Measurement Model

The systems of the International Laser Ranging Service (ILRS) provide millimeter accuracy range observations by measuring the transit time of pulsed laser returns from retro-reflectors carried by the spacecraft. The measurements are calibrated for known instrument characteristics and for the effects of atmospheric refraction in order to use them for ultra-precise orbit determination.

The laser range measurement is the transit time of a pulse of laser light measured from the time it is emitted by the laser at t_0 to the time when it is received in a detector at the laser station, t_2. The pulse is reflected from a retro-reflector on the spacecraft at an intermediate time, t_1. The range to the spacecraft can then be computed by dividing the total time by two and multiplying by the speed of light, c.

The model used by GEODYN to calculate this range is:

$$R = \frac{1}{2}\left[\left(\vec{r}_{sat}(t_1) - \vec{r}_{sta}(t_0)\right)^2 + \left(\vec{r}_{sta}(t_2) - \vec{r}_{sat}(t_1)\right)^2\right]^{\frac{1}{2}} \qquad (9.4.1.1)$$

where

R is the calculated laser range

$\vec{r}_{sat}(t)$ is the inertial position vector of the satellite at time t

$\vec{r}_{sta}(t)$ is the inertial position vector of the station at time t

t_0, t_1, t_2 are the times defined above

The partial derivatives of the laser range are:

$$\frac{\partial R}{\partial\left(r_{sat}\right)_i} = \frac{\left(r_{sat}\right)_i}{R} = -\frac{\partial R}{\partial\left(r_{sta}\right)_i} \qquad (9.4.1.2)$$

where

$(r_{sat})_i$ are the inertial components of the satellite

$(r_{sta})_i$ are the inertial components of the station.

9.4.2 GPS Measurement Model

The Global Positioning System space segment comprises at least 24 satellites in six orbital planes at inclinations of 55 degrees and at 20,200 km altitude. The GPS constellation can be used to locate a receiver on the ground or in-flight in a reference system defined by the orbits provided by the International GNSS Service (IGS). The GPS constellation is a component of GNSS (Global Navigation Satellite Systems). A dual-frequency receiver carried by the spacecraft provides satellite-to-satellite tracking measurements of pseudorange and carrier phase.

9.4.2.1 Code Pseudorange

Code pseudorange is derived from the transit time of coded radio-frequency signals broadcast by the GPS satellites and recorded by GPS receivers. Two grades of noise codes modulate the carrier signals at the L1 and L2 frequencies. A civilian access (C/A) code has a chip-rate of about 1 MHz and can be used to generate ten-meter range measurements. The precise P-code can produce ranges accurate to better than one meter, with a 10 MHz chip-rate, and can be used in

conjunction with the C/A code measurements to recover the first-order ionospheric propagation delay.

The code pseudorange measurement can be expressed by:

$$R_c = c\Delta t + c\Delta\delta + \Delta r_{tropo} + \Delta r_{iono} + \Delta r_{rel} \qquad (9.4.2.1.1)$$

Where

R_c	is the code pseudorange
Δt	is the transit time difference
$\Delta\delta$	is the difference of the station and satellite clock errors
c	is the speed of light
Δr_{tropo}	is the tropospheric range error
Δr_{iono}	is the ionospheric range error (absolute value)
Δr_{rel}	is the correction for relativistic effects

9.4.2.2 Phase Pseudorange

Phase pseudorange measurements are formed by tracking the phase changes of the GPS carrier signal over an interval of time. The change in phase during the time interval translates directly into the change in range during the interval. The highly stable oscillators on board the GPS satellites also allow the use of the carrier to be used for ranging at the millimeter level.

There are several problems with the phase measurement, chiefly, cycle slip errors and errors in the satellite and receiver clocks. If a GPS receiver loses phase lock on a signal, when the signal is re-acquired the phase will have changed by an unknown amount. This event is known as a cycle slip. Unless some method of removing cycle slips is employed, the length of a phase tracking arc is limited to the interval between cycle slips.

The phase pseudorange measurement can be expressed as:

$$R_p = \Phi\lambda = \rho + c\Delta\delta + N\lambda + \Delta r_{tropo} - \Delta r_{iono} \qquad (9.4.2.2.1)$$

where

R_p	is the phase pseudorange
Φ	is the carrier phase
ρ	is the true range

$\Delta\delta$ is the difference of the station and satellite clock errors

c is the speed of light

λ is the carrier wavelength

N is the phase ambiguity, an integer number of cycles

Δr_{tropo} is the tropospheric range error

Δr_{iono} is the ionospheric range error (absolute value)

Notice that the sign of the ionospheric error in the phase measurement is opposite to the sign of the ionospheric error in the code measurement.

9.4.2.3 Single and Double Differences

In order to attempt to eliminate the first order effects of GPS satellite clock error and selective availability, single differences of carrier phase observations are made by differencing two carrier phase ranges to the user satellite from two different GPS satellites. The single differences formed in this manner do not, however, remove the clock errors in the user satellite clock or GPS receiver, which may be larger than the GPS clock errors. For this reason, most satellite orbit determination using GPS uses double differences of range observables, which remove satellite clock errors.

GPS data collected on the spacecraft are combined with GPS data from ground receivers to form doubly differenced ambiguous one-way ranges. The double differences remove the first order effects of the large receiver clock errors, smaller GPS clock errors, and selective availability from the observation, at the cost of some geometrical information. The remaining second order effects of clock error appear mainly as time tag errors [*Rowlands, et al., 1997*].

The GEODYN system can use either single or double difference one-way ranges alone or in combination to determine the orbit.

Consider first the single difference of measurements from one satellite to two stations. The clock errors in the measurements can be written:

$$\Delta\delta = \delta_{sat} - \delta_{sta} \qquad (9.4.2.3.1)$$

where δ_{sat} and δ_{sta} represent the independent clock errors in the satellite clock and the station clock, respectively. The two measurements can be written:

$$R_A^j(t) = \rho_A^j(t) + \lambda N_A^j + c\delta^j(t) - c\delta_A(t) + \left(r_{tropo}\right)_A^j + \left(r_{iono}\right)_A^j$$
$$R_B^j(t) = \rho_B^j(t) + \lambda N_B^j + c\delta^j(t) - c\delta_B(t) + \left(r_{tropo}\right)_B^j + \left(r_{iono}\right)_B^j \qquad (9.4.2.3.2)$$

for measurements between satellite *j* and stations *A* and *B*, taken at time *t*. Differencing these equations eliminates the $c\delta$ term, and, if the substitution $Q_A - Q_B \rightarrow Q_{AB}$ is made, the resulting equation is:

$$R_{AB}^j(t) = \rho_{AB}^j(t) + \lambda N_{AB}^j - c\delta_{AB}(t) + \left(r_{tropo}\right)_{AB}^j + \left(r_{iono}\right)_{AB}^j \qquad (9.4.2.3.3)$$

The difference has eliminated the satellite clock error.

If the above single difference equation for satellite *j* is differenced with the corresponding equation for satellite *k*, the result is a double difference measurement. Using the substitution $Q^j - Q^k \rightarrow Q^{jk}$,

the result is:

$$R_{AB}^{jk}(t) = \rho_{AB}^{jk}(t) + \lambda N_{AB}^{jk} + \left(r_{tropo}\right)_{AB}^{jk} + \left(r_{iono}\right)_{AB}^{jk} \qquad (9.4.2.3.4)$$

and the station clock errors have been eliminated. There still remains the ambiguity term, which must be solved for as a bias, and the tropospheric and ionospheric errors. As discussed below, the tropospheric and ionospheric corrections can be modeled, and it is likely that there will be some cancellation in these atmospheric effects. If the double differences are computed from single measurements that are not taken simultaneously, then the clock error cancellation is not complete, and second-order clock errors due to clock drifts remain in the double difference measurement.

9.4.2.4 GPS Satellite Yaw-Attitude Model

Significant improvements have been made in the yaw-attitude modeling of GPS satellites, particularly during eclipse periods. The three types of GPS satellites that are modeled are Block IIA, IIF, and IIR satellites. The four distinct time periods for which the yaw-attitude is modeled are nominal periods, noon turns, midnight turns (shadow crossing), and post-shadow recovery periods. The current model being implemented is given by [Kouba, 2009; Kouba, 2013]. This model can accurately predict the yaw-attitude for all satellites and during all periods given above, with the exception of post-shadow recovery periods of Block IIA satellites.

The table below presents a summary of the expected satellite motion during each of the distinct periods listed above. The expected motion is oftentimes dependent on the beta angle, which is the acute angle between the Sun vector and the orbit plane (positive if Sun vector forms an acute and with orbit normal, negative otherwise). For exact formulas, refer to the literature given by [Kouba, 2009; Kouba, 2013] and [Bar-Sever, 1996]. Note in the table below that YBIAS

represents the effective yaw-bias of GPS satellite. For Block IIA satellites, YBIAS is approximately +0.9°. For Block IIF satellites, YBIAS is approximately -0.9°. The nominal yaw-bias values for Block IIA and IIF satellites are +0.5° and -0.5°, respectively.

	Nominal Period	**Noon Turn**	**Midnight Turn**	**Post-Shadow Recovery**
Block IIA Satellites	Follows nominal yaw-attitude: Navigation antenna points toward Earth Normal to solar array surface points at Sun	Attempts to follow nominal orientation When nominal yaw-rate exceeds max hardware rate (~0.13°/s), satellite turns at max rate until yaw-angle "catches up" with nominal **For β<0°, β>YBIAS: satellite turns in <u>same</u> direction as the nominal** **For 0°<β<YBIAS: satellite turns in <u>opposite</u> direction as the nominal**	Starts turning, upon shadow entry, at the maximum hardware rate in the positive direction (due to positive yaw-bias)	Turns at maximum hardware rate in an attempt to return to nominal orientation **RECOVERY DIRECTION IS UNKNOWN!**
Block IIR Satellites	Follows nominal yaw-attitude: Navigation antenna points toward Earth Normal to solar array surface points at Sun	Attempts to follow nominal orientation When nominal yaw-rate exceeds max hardware rate (~0.20°/s), satellite turns at max rate until yaw-angle "catches up" with nominal	Satellite maintains nominal yaw-orientation during midnight turn and only performs a turn, analogous to a midnight maneuver, when it cannot keep up with the nominal orientation	None: satellite exits midnight turn in nominal orientation
Block IIF Satellites	Follows nominal yaw-attitude: Navigation antenna points toward Earth Normal to solar array surface points at Sun	Attempts to follow nominal orientation When nominal yaw-rate exceeds max hardware rate (~0.11°/s), satellite turns at max rate until yaw-angle "catches up" with nominal **For β<YBIAS, β>0°: satellite turns in <u>same</u> direction as the nominal** **For YBIAS<β<0°: satellite turns in <u>opposite</u> direction as the nominal**	For |β|>8°: satellite maintains nominal yaw-orientation during shadow crossing and only performs a turn, analogous to a noon turn maneuver, when it cannot keep up with the nominal orientation For |β|<8°: satellite turns in required direction at constant rate of 0.06°/s	Satellite turns at maximum hardware rate (~0.11°/s) until the nominal orientation is recovered (takes < 5 minutes)

The exact effective yaw-bias values of GPS satellites are unknown. Because of this, the above model may also be inaccurate during noon turn maneuvers of Block IIA and IIF satellites when the β angle is close to the yaw-bias value. For this reason, data will be deleted from Block IIA and IIF satellites undergoing noon turn maneuvers when the β angle is between the nominal and effective yaw-bias value or within +/- 0.1° of either value. In summary, the yaw-attitude model for GPS satellites given by [Kouba, 2009; Kouba, 2013] will be implemented. The three cases where the model will not be trusted, and the associated data will be deleted, are listed below:

- Post-shadow recovery periods (30 minutes) of Block IIA satellites following midnight turns longer in duration than 15 minutes
- Noon turn maneuvers of Block IIA satellites where $0.4° < \beta < 1.0°$
- Noon turn maneuvers of Block IIF satellites where $-1.0° < \beta < -0.4°$

9.4.2.5 Reverse Kinematic Software

In addition to the yaw-attitude modeling improvements given above, a reverse-kinematic software package is being developed and tested. This software will be able to provide an alternative yaw-attitude solution for GPS satellites, which can be used during periods when the yaw-attitude model described above may be incorrect (and the data would otherwise be deleted). Preliminary tests show that this may be a valuable tool. Currently, a method for determining the quality of a reverse-kinematic solution is being developed, and work is also being done to incorporate it alongside GEODYN.

9.4.2.6 IGS Tracking Station Selection

New software has been developed for selecting an optimal set of IGS tracking stations to be used for GPS data processing. Stations will be selected from the IGS "core stations" list, currently consisting of 194 stations, as recommended by the IGS during their 2nd reprocessing campaign. This core stations list is broken up into subsets, each consisting of a primary station and up to four nearby alternative stations. The most recent version released by the IGS consists of 91 core station subsets.

To start, each station on the core station list is checked to see if it should be eligible for selection. The two reasons that a station may be automatically eliminated from contention is if it has no data available over the time period input to the software or if there is an earthquake-related discontinuity in the station's solution that occurred prior to or during the time period input. From there, a preliminary list of stations to select from is created, choosing up to one station from each of the core station subsets. If the primary station from a subset is a candidate for selection, that station is added to the list. If not, the alternative stations are checked to see if they are still candidates for selection. The first alternative station found that is still a candidate for selection, assuming there is one, is then added to the list. This creates a list of stations, up to the number of core station subsets, from which the final list of stations and hub stations will be selected.

The optimization procedure run later to select the final set of stations bases its selection of the final stations on two criteria: data availability for each station and geographic coverage of a set of stations. For each station, two criteria are used to compute a data availability score by looking only at the time period input to the software: the number of days over the time period where no data was available and the percentage of actual observations (out of the number expected) for days in which some data was available. It is preferred to have stations with infrequent periods where data is missing as opposed to full days. As such, a relative weighting factor, δ, is used to specify the desired relative weighting between the criteria that go into computing each station's score. The exact formula used is:

$$Score = \delta * x + (1 - \delta) * y$$

Where *x* is the percentage of days with data available, and *y* is the percentage of observations (out of the number expected) for days in which some amount of data is available. The weighting factor, δ, must be a number between 0 and 1, likely greater than 0.5 because it is desired to avoid selecting stations that are missing full days worth of data.

The optimization procedure then selects the best final set of stations. It does so by computing a cost for any given set of stations. As such, it begins by assuming a set of stations equal to the number of desired stations and computes a cost for this set. It then attempts to swap in other stations to the final list, checking to see if the cost is reduced, and making a switch permanent if the cost is made lower. This process continues until the minimal cost is found.

The total cost is computed as the sum of a distance cost and a score cost, with each being weighted appropriately using a weighting factor, λ. The formula used is:

$$Cost = \frac{1}{\lambda * \frac{1}{(Distance\ Cost)} + (1 - \lambda) * \frac{1}{(Score\ Cost)}}$$

When λ is equal to 1, the optimization is based solely on distance (geographic coverage). When λ is equal to 0, the optimization is based solely on score (data availability). The distance and score costs are computed as follows:

$$Distance\ Cost = \frac{1}{(Sum\ Distances) * (Optimal\ Distance\ Cost)}$$

$$Score\ Cost = \frac{1}{(Sum\ Scores) * (Optimal\ Score\ Cost)}$$

In the above formulas, the sum of the distances is the sum over all stations in the set of the distance to its nearest neighboring stations (computed using the Haversine formula) and the sum of the scores is the sum over all stations in the set of the scores given to them based on their data availability. It's true for both distance and score that the higher these sums are the better. And it can be seen from the above formulas that in both cases this also leads to a lower cost, as is desired.

The optimal costs for both distance and score are used to normalize the two selection criteria. As such the optimization code must be run three times:

- Once with λ equals 1 to compute the optimal distance cost
- Once with λ equals 0 to compute the optimal score cost
- Once with λ equals the value input by the user to determine the optimal final cost

The optimal distance and score costs are initialized to 1 and the updated after the 1st and 2nd runs of the optimization code, respectively. The set of stations associated with the optimal final cost determined during the 3rd run of the optimization code is the final set of selected stations that is output by the station selection software.

It has been found that a different method than was used to select the final stations is needed for selecting the hub stations. The hub stations should be comprised of the best, most consistently tracking stations, and should therefore remain similar from year to year. The following method is therefore used to select the hub stations.

Information for each station on the core list for the entire period it was tracking data (not just the time period input to the software to base its selection off of) is first read in from a previously created file. This information includes the total number of days between the first and last days the station was tracking, the number of days over that time period for which data is available, the number of days over that time period for which data is unavailable, and the percentage of observations out for the expected number for days where data is available. This information is used to compute an overall score for each station using the same formula and value for δ that was used previously to compute the regular scores. It will be that case that each station will have the same overall score for different runs of the station selection software, assuming the same value of δ is used. This consistency of the overall scores between runs will be utilized to obtain better consistency amongst the hub stations selected when various time periods are input to the software.

Only stations that have been selected to the final list of stations are eligible to be chosen as hub stations. The overall scores will be used as follows to select the hub stations from this list. First, the station with the highest overall score is chosen as a hub. Then, the station with the 2nd highest overall score is checked to see if the minimum distance from itself to any of the already selected

hub stations is greater than a pre-specified value. If it is (meaning it is deemed to be far enough away from all other hub stations), then it is selected as a hub station. If not, it is skipped. This process continues, always checking the station with the next highest overall score, until the desired number of hub stations have been selected. If the software goes through all stations that are eligible to be selected as hub stations and the desired number has still not been reached (meaning the minimum distance requirement between all hub stations could not be met), then it will simply add the stations with the next highest overall scores (regardless of their location) until the desired number is reached.

The station selection software treats the Earth as a sphere of radius 1, for reasons of simplicity. The maximum geodetic distance therefore, between two stations on the opposite side of the globe, is π. It has been found that using π/4 as the minimum allowable distance between hub stations works well, although it is also dependent on the desired number of hub stations. Lowering the minimum distance value will help to select the best performing set of hub stations with the highest overall scores, while raising it will help improve the geographic coverage of the set (assuming the minimum distance requirement can still be met for all stations). Final tuning of the weighting parameters discussed above as well as this minimum distance between the hub stations value is still to be completed.

9.4.2.7 Gravitational Delay

The gravitational delay due to the presence of the Earth will be modeled for GPS signals received by the ICESat-2 spacecraft. Let x_1 be the coordinate where the signal is emitted, x_2 be the coordinate where the signal is received, and x_J be the coordinate of the center of mass of the Earth. Then, as derived from equation (11.17) of the IERS2010 Conventions document, the gravitation delay can be computed as:

$$\Delta t = \frac{2GM}{c^3} \ln\left(\frac{r_{J1} + r_{J2} + \rho}{r_{J1} + r_{J2} - \rho}\right)$$

Where $r_{J1} = \left|\vec{x}_1 - \vec{x}_J\right|$, $r_{J2} = \left|\vec{x}_2 - \vec{x}_J\right|$, and $\rho = |\vec{x}_2 - \vec{x}_1|$.

9.4.3 Laser Altimeter Measurement Model

The laser altimeter measurements will in all likelihood not be a part of the operational precision orbit determination process, provided proper functionality of the ICESat-2 GPS receiver. However, in the absence of GPS tracking data, the laser altimeter measurement can be utilized to determine the orbit, though with less accuracy than with the GPS data. The laser altimeter measurements will be a key component to the calibration and validation activities (see Section 5.3), which are crucial in detecting any systematic errors in the orbit determination and assessing the orbit accuracy.

The material presented in this section is also contained in the Geolocation Parameter Estimation; Pointing Calibration section of the ICESat-2 Calibration/Validation ATBD.

9.4.3.1 Direct Laser Altimeter Range Processing

The laser range is quite sensitive to pointing errors as seen from the following expression (using the same notation as previously presented):

$$\sigma_\rho = \frac{z \tan\theta}{\cos\theta}\sigma_\theta \qquad (9.4.3.1.1)$$

Therefore, the direct altimetry is potentially an excellent data type to observe and remove pointing errors in addition to S/C positioning and instrument bias errors.

When direct altimetry is processed, GEODYN compares observed altimetry ranges to those that are computed internally (measurement model). As with any tracking data type, the discrepancies between the observed and computed observations (i.e. the residuals) are minimized by adjusting parameters that affect the computed observation. Unlike any other tracking data type (except crossovers) direct altimetry involves a "bounce point" which does not occur at a satellite or at a fixed tracking station. For direct altimetry unlike crossovers, the bounce point location must be computed using some knowledge of the planet's surface. This is due to the fact that the bounce point is approximated by determining where the laser would intersect the planet's ellipsoid. Sloping surface topography is an additional complication which is eliminated when using a crossover technique. However, for ocean data, models exist which accurately describe the surface topography. For continental surfaces, a topographic model is also used but with far less certainty compared to the current ocean model capabilities.

The following algorithm description derives many of its parameters from the ATL03g ICESat-2 Receive Photon Geolocation ATBD.

9.4.3.2 Direct Laser Altimeter Range Measurement Model

The optical center and the pointing of the laser altimeter are both computed in the CRF at instrument transmit time as described in the Geolocation ATBD.

$$\vec{X}^T_{OP} = \vec{X}^T_{S/C} + \vec{x}^T_{cmoff} \qquad \hat{p} = R^T_{SBF\rightarrow CRF} R^T_{Laser\rightarrow SBF} \begin{bmatrix} 0 \\ 0 \\ -1 \end{bmatrix} \qquad (9.4.3.2.1)$$

The optical center and the pointing are then rotated to the ECF frame following Section ??? of the ATL03g ICESat-2 Receive Photon Geolocation ATBD.

The direction cosines of the ECF pointing unit vector are used to form the equation of a line with respect to the ECF. Coupled with the equation of an ellipse we can then solve for the intersection of the observation line of sight with the ellipsoid.

Equation of line $\frac{x-x'}{\cos\alpha}=\frac{y-y'}{\cos\beta}=\frac{z-z'}{\cos\gamma}$ (9.4.3.2.2)

where:

x, y, z	Are coordinates of $\vec{X}^T_{OP(ECF)}$
x', y', z'	are the coordinates of the intersection of the observation line of sight and the ellipsoid
$\cos\alpha,\cos\beta,\cos\gamma$	are the direction cosines of the unit pointing vector in ECF x, y, and z

The equation of the ellipse where a and b are the semi-major and semi-minor axis is:

$$\frac{x'^2+y'^2}{a^2}+\frac{z'^2}{b^2}=1 \qquad (9.4.3.2.3)$$

Then solving for x' and y' of the ellipse intersection:

$$x'=x-\frac{z-z'}{\cos\gamma}\cos\alpha \qquad y'=y-\frac{z-z'}{\cos\gamma}\cos\beta \qquad (9.4.3.2.4)$$

Substituting the above into the equation of the ellipse and normalizing all distances by the semiminor axis such that b=1 gives:

$$\left[x\cos\gamma-\left(z-z'\right)\cos\alpha\right]^2+\left[y\cos\gamma-(z-z')\cos\beta\right]^2+a^2\cos^2\gamma\left(z'^2-1\right)=0 \qquad (9.4.3.2.5)$$

This equation is then solved for z'. Once z' is computed x' and y' are then computed from the relationships above.

The ellipsoid intersection is then used as the first guess location of the altimeter bounce point $\vec{X}^B_{B(ECF)}$.

1) The bounce point time is computed for site displacement modeling using the corrections for atmospheric refraction as described in Section 3.1, Step 1, ATL03g ICESat-2 Receive Photon Geolocation ATBD:

$$T_B=T_T+\frac{\left|\vec{X}^T_{OP(ECF)}-\vec{X}^B_{B(ECF)}\right|+\Delta\rho_{atm}}{c} \qquad (9.4.3.2.6)$$

Geodetic coordinates are then computed (as in Section 3.1, Step 8, ATL03g ICESat-2 Receive Photon Geolocation ATBD) from the ellipsoid intersection. These geodetic coordinates are used to compute the surface at that location including site displacement effects:

$$\vec{X}_{S(ECF)} = \vec{x}_S + \vec{x}^B_{ET} + \vec{x}^B_{PT} + \vec{x}^B_{CM} + \vec{x}^B_{OL} + \vec{x}^B_{OT} \qquad (9.4.3.2.7)$$

$\vec{x}_s$ surface location as described by surface model

The distance between the surface and the first guess bounce point is then computed:

$$d = \left| \vec{X}_{S(ECF)} - X^B_{B(ECF)} \right| \qquad (9.4.3.2.8)$$

If d has converged (i.e. d is less than some ε) then the bounce point location and time have been found. If not, then a new bounce point guess is computed as follows, and iterated till convergence.

$$\vec{X}^B_{B(ECF)} = \vec{X}^B_{B(ECF)} - d(-\hat{p}) \qquad (9.4.3.2.9)$$

The geometric transmit leg range is then computed using the converged bounce point:

$$\rho_T = \left| \vec{X}^T_{OP(ECF)} - \vec{X}^B_{B(ECF)} \right| \qquad (9.4.3.2.10)$$

Now, the receive S/C position in CRF using an iterative light time solution, with the CRF bounce point position, is computed where the first guess of the receive time is

$$T_R = T_T + 2(\rho_T + \Delta\rho_{atm}) \qquad (9.4.3.2.11)$$

Once converged, the optical center of the instrument at T_R is then computed as

$$\vec{X}^R_{OP} = \vec{X}^R_{S/C} + \vec{x}^R_{cmoff} \qquad (9.4.3.2.12)$$

The above is rotated to ECF and the observed laser one-way range is then computed as:

$$\rho = \frac{\left| \vec{X}^R_{OP(ECF)} - \vec{X}^B_{B(ECF)} \right| + \rho_T}{2} + \Delta\rho_{atm} + \Delta\rho_{bias} \qquad (9.4.3.2.13)$$

The partial derivatives of the range measurement with respect to the S/C position and range biases are rigorously computed from the equation above. The partials of the measurement with respect to S/C attitude corrections and laser pointing are numerical approximated due to the additional complexity of the surface model. The formulation for the pointing related parameterization is given in the next section.

9.4.3.3 Spacecraft Attitude Correction and Laser Pointing Parameterization

The overall pointing of the laser altimeter is modeled in GEODYN with a succession of rotation matrices denoted by *R*. Therefore the pointing in the CRF is represented as (see Section 3.1, Step 4, ATL03g ICESat-2 Receive Photon Geolocation ATBD):

$$\hat{p} = R^T_{SBF\rightarrow CRF} R^T_{SBFC\rightarrow SBF} R^T_{Laser\rightarrow SBFC} \begin{bmatrix} 0 \\ 0 \\ -1 \end{bmatrix} \qquad (9.4.3.3.1)$$

where

$R^T_{Laser\rightarrow SBFC}$ is the rotation from the laser frame to the corrected SBF at *TT*

$R^T_{SBFC\rightarrow SBF}$ is the rotation from the corrected SBF to the SBF at *TT*

$R^T_{SBF\rightarrow CRF}$ is the rotation from the SBF frame to the CRF at *TT*

$\begin{bmatrix} 0 \\ 0 \\ -1 \end{bmatrix}$ is the convention used for the laser emission pointing in the laser frame

The SBF-to-CRF rotation is provided by the spacecraft ADACS, while the first two rotation matrices are specified by the user with a 3 axis Euler rotation in roll, pitch and yaw. The Euler angle representation was chosen for the parameterization since it is much more intuitive than a quaternion representation and, since the user has the flexibility to select the order of rotation, any singularities may be avoided. The SBFC-to-SBF matrix is provided to facilitate the capability to estimate a correction to the telemetered S/C attitude (SBF-to-CRF). If no correction is needed then this is simply the identity matrix. GEODYN has the capability to model N number of Laser-to-SBF rotation matrices for N number of lasers composing the complete instrument. Only one SBFC-to-SBF matrix may be modeled. Thus, the Laser-to-SBFC and the SBFC-to-SBF rotation matrices are constructed using roll, pitch and yaw parameterized in the following manner:

$$\begin{aligned} roll &= C_r + R_r\Delta t + Q_r\Delta t^2 + A_r \sin\omega t + B_r \cos\omega t \\ pitch &= C_p + R_p\Delta t + Q_p\Delta t^2 + A_p \sin\omega t + B_p \cos\omega t \\ yaw &= C_y + R_y\Delta t + Q_y\Delta t^2 + A_y \sin\omega t + B_y \cos\omega t \end{aligned} \qquad (9.4.3.3.2)$$

The parameterization is time dependent, which means the user may select this parameterization for as many time periods (with user defined length) as desired. The time dependent

parameterization provides a powerful tool when trying to model/estimate pointing errors induced by thermal cycling of the instrument.

This parameterization can be modified to compensate for additional error signatures.

The partial derivatives of the direct altimeter range measurement with respect to each of the parameters of roll, pitch, and yaw (C, R, Q, A, B) are computed by: (1) rigorously computing the partials of roll, pitch and yaw with respect to the parameters and (2) chaining these partials with the numerically computed partials of the measurement with respect to roll, pitch and yaw.

9.4.3.4 Laser Altimeter Dynamic Crossovers

Unlike any other tracking data type, direct altimetry is sensitive to parameters, which describe the planet's surface. This sensitivity can be overcome with accurate surface models (*i.e.* ocean surface models derived from the latest ocean altimeter missions) or can be an advantage if the goal is to refine parameters, which describe the surface. However, the surface model dependence of the direct altimetry can also be a distinct disadvantage since many areas of the Earth (land and coastal regions) are poorly modeled at the level necessary to improve the pointing knowledge. Therefore, crossovers provide a distinct advantage since they require no knowledge of the dominant time-independent part of the surface topography.

GEODYN uses tracking data observations to form least squares observation equations. The one exception to this rule is the altimeter crossover data type. Each crossover is a pair of direct altimetry ranges that are used in the same least squares constraint equation. The idea is as follows. Forming the crossover difference removes any dependence on the static topographic features associated with a precise geographic location. Now, instead of computing where bounce points occur as in direct altimetry, the bounce points are located by "hanging" the observations from the computed satellite ephemeris. The ascending and descending ground tracks of a satellite must intersect. The "hung" altimeter bounce points of the ascending and descending passes trace out three dimensional curves on the planet's instantaneous surface that roughly correspond to the ground tracks. If these curves are corrected to remove time varying surface effects like tides, they too should intersect. In practice they do not quite intersect. This misclosure is due to observation noise, but also errors in the satellite ephemeris and in attitude as well as in tidal models. A constraint equation is written for each crossover pair to cause adjusting parameters to minimize crossover discrepancies overall. Notice that no knowledge of the planet surface other than tidal behavior is required.

Conventional crossover processing uses some simplifying assumptions:

- The altimeter points geodetically with no pointing error. In other words, the geodetic latitude of the point where the altimeter ray intersects the ellipsoid is the same as the geodetic latitude of the satellite.
- At the data preprocessing stage (before the orbit determination process has been started), the satellite ephemeris is already known well enough in the along track and cross track components to predetermine:

- The latitude of crossover points
- The longitude of crossover points
- Which observations belong in each crossover pair

With these assumptions, the crossover constraint equations are quite straightforward. The constraint equation essentially forces the difference between satellite heights (above the ellipsoid) at the two times of the crossover to equal the difference between altimeter ranges at the two times of the crossover. Tidal effects are accounted for using models and eliminated when forming the difference. Conventional crossovers are useful for determining the orbital parameters that affect the radial component of the ephemeris and also for the determination of tidal parameters through identification of differences at prescribed temporal periodicities.

It should be noted that conventional crossovers have been used mainly over oceans and with radar (not laser) altimetry. In such cases the above simplifying assumptions are adequate even for very precise experiments.

When acquiring ocean returns and over very smooth topographic surfaces, altimeter range measurements can be interpolated to the crossover location in order to compute this difference. In principle, forming such a difference removes static effects (such as topography and geoid height) at the location, leaving the computed *vs*. observed height difference as a measure of errors in modeling the orbit position and for laser altimetry, satellite orientation as the dominant misclosure signal. When over oceans, errors in modeling the tides, dynamic topography, and other effects such as sea state will also contribute to the crossover difference. Thus with today's improvements in modeling the ocean surface effects, it is possible to recover the orbit position and satellite orientation by solving for appropriate corrections within these models from the crossover data.

Unlike radar altimeter system where it is known that the sub-satellite nadir looking point is being ranged to, laser altimeter observations illuminate a spot on the surface which is very much dependent on satellite attitude and instrument pointing. These instrument and satellite models themselves can be improved within a data reduction setting, but this often means given the high data rate offered by these systems, that the pair of observations forming a crossover measurement will change as these attitude and pointing models are refined. To accommodate improvements to these satellite attitude and pointing models, GEODYN has been enhanced so that the crossover pairs are recomputed/matched on each iteration of the estimation process. Such observation pairs are called dynamic crossovers [*Rowlands et al. 1999*].

Within dynamic crossovers, the exact latitude, longitude and times of the observations that define each crossover are not predetermined. For dynamic crossovers these are computed during the orbit determination process based on the latest values of orbit and attitude parameters. Orbit determination is an iterative process due to the nonlinear nature of the parameters being estimated. The location of each crossover is allowed to change on each iteration based on the values of parameters in that iteration. As parameter values converge, so will crossover locations.

Another enhancement of dynamic crossovers is that the constraint equations are not restricted to the radial direction. The constraint equations of dynamic crossovers are written to minimize the (minimum) distance between the three dimensional curves that are traced out by the geolocated and tidally corrected altimetry. The nature of these new constraint equations is consistent with the approach that crossover locations are not predetermined. In order to minimize the minimum distance between two curves, it is necessary to consider more than one data point on each curve. Also, if exact crossover locations are not predetermined, then it is necessary to consider more than one direct altimetry observation for each half of each crossover. Each dynamic crossover consists of a pair of direct altimetry streams (sequence of adjacent observations).

GEODYN and its crossover preprocessing software have undergone extensive modifications for the dynamic crossover capability. The crossover preprocessing software still pre-computes locations and times of crossovers. However these locations and times are now understood to be approximate. The crossover preprocessor identifies direct altimetry observations that are close to crossover (minimum distance) locations. All such direct altimetry observations are passed to GEODYN.

In GEODYN, the measurement modeling follows this general scheme. On a given estimation inner iteration, the current estimate of parameters together with the observed altimeter range is used to geolocate each bounce point of the direct altimetry streams in space (see Section 3.1, Step 5, ATL03g ICESat-2 Receive Photon Geolocation ATBD). What will have been determined are a series of coordinates that describe the observed surface of the Earth or a surface connected to the Earth. Those coordinates are corrected for tides and other time varying effects. At this point each stream of direct altimetry describes a curve on a mean (more or less time invariant) surface on or connected to the Earth. The streams of coordinates as well as the partial derivatives of these coordinates with respect to all adjusting parameters are stored off for use in observation equation processing.

The observation equations are used to minimize the (minimum) distance between the observed mean surface curves that correspond to each of the pairs of altimetry streams of each crossover. Note that we are using the observations to find the mean surface curves. When this approach is used, there is no guarantee that the mean surface curves will intersect.

Each stream of X coordinates of these observed mean surface curves are fit to its own polynomial and, of course, the same is done for the Y and Z coordinates. The (minimum) distance between each of the two triplicates of polynomials of each crossover can be computed. That distance (which should be zero in the absence of noise and parameter error) is the residual of the observation/constraint equation.

Each X coordinate in a stream affects the equation of the X polynomial of the stream and the analogous statement applies for each Y and Z coordinate. Therefore, the partial derivative of the (minimum) distance between the two triplicates of polynomials with respect to each X, Y and Z coordinate in each of the two streams can be computed. As stated above, the partial derivative of these coordinates with respect to each adjusting parameter have already been computed and stored off. Using the chain rule, the partial derivative of the (minimum) distance between the two

triplicates of polynomials with respect to each adjusting parameter can also be computed. The information needed for an adjustment is thereby defined.

9.4.4 Ground Station and Bounce Point Displacement

This section outlines the Earth surface displacements that should be applied as corrections to the GPS ground station positions and the laser altimeter range measurements. The total surface displacement corrections over land and ocean are described by:

$$\Delta_{land} = \Delta_{Earth\ tide} + \Delta_{ocean\ loading} + \Delta_{pole\ tide} + \Delta_{geocenter}$$
$$\Delta_{ocean} = \Delta_{Earth\ tide} + \Delta_{ocean\ tide} + \Delta_{load\ tide} + \Delta_{atm\ loading} + \Delta_{pole\ tide} + \Delta_{geocenter} \quad (9.4.4.1)$$

where

$\Delta_{Earth\ tide}$ = displacement due to solid Earth tides

$\Delta_{ocean\ tide}$ = displacement due to ocean tides

$\Delta_{load\ tide}$ = solid Earth displacement due to overlying ocean tides

$\Delta_{ocean\ loading}$ = solid Earth displacement over land due to ocean loading

$\Delta_{pole\ tide}$ = rotational deformation due to polar motion

$\Delta_{atm\ loading}$ = ocean response to atmospheric loading

$\Delta_{geocenter}$ = effect of geocenter motion

Each of these components is discussed below.

This section discusses the Earth surface displacements that occur due to tidal effects and atmospheric loading. The models of these time-variable surface displacements must be applied to the GPS ground stations, and must be accounted for when processing the laser altimeter measurements.

9.4.4.1 Solid-Earth Body Tide Correction

The Earth's body tide is modeled as a purely elastic response to the lunar and solar tidal potentials. The algorithm described below is identical to that used for the T/P GDR data, and is used for all altimeter satellites in order to maintain consistency with the ocean-tide models, which largely depend on T/P data.

The lunar and solar tidal potentials are computed from the semi-numerical expansion of Cartwright and Taylor, described by [*Cartwright and Edden, 1973*], extrapolated linearly to the defined epoch (*i.e.* the Pathfinder developed model uses 1990 for its epoch). The complete expansion is used, with terms of both second and third degrees in the potential. Only the first term, from the permanent tide has not been used. By agreement (within the T/P Science

Working Group), the permanent tide is included in the geoid model (*i.e.* contained within the J_2 harmonic).

The body-tide vertical displacement depends on the adopted h_2 and h_3 Love numbers. For the T/P and Pathfinder projects, the following Love numbers were adopted:

$h_2 = 0.609$ for all terms of degree 2, except

$= 0.5203$ for the K_1 tide and its nodal sidelines.

$h_3 = 0.291$ for all terms of degree 3.

These values will be used herein. These terms are approximately those computed by [*Wahr, 1981*], with the exception that Wahr found $h_2 = 0.606$ for long-period tides and a much more complex behavior in the diurnal band surrounding the nearly-diurnal free-wobble frequency. Also, all latitude dependence in the Love numbers has been neglected. As noted above, however, we have followed the T/P algorithm for consistency with the ocean tide models

An important effect of the solid tide is the displacement of the tracking stations caused by this tide. The displacement is also an important correction for the instantaneous height of the altimeter source point, and is calculated in the same manner as the displacement of the tracking stations. This correction can be computed from Wahr's theory, where only the second-degree tides are needed for centimeter level precision [*Project Merit Standards, 1983, and McCarthy, 1996*]. The formulation used in GEODYN uses the frequency independent Love and Shida numbers and a derivation of the tidal potential in the time domain. The formula used in GEODYN for the vector displacement of the station [*Diamante and Williamson*, 1972] is:

$$\Delta\vec{r} = \sum_{j=1}^{2}\left[\frac{GM_j}{GM_\oplus}\frac{r^4}{R_j^3}\right]\left\{\left[3l_2\left(\hat{R}_j\cdot\hat{r}\right)\right]\hat{R}_j + \left[3\left(\frac{h_2}{2}-l_2\right)\left(\hat{R}_j\cdot\hat{r}\right)^2 - \frac{h_2}{2}\right]\hat{r}\right\} \qquad (9.4.4.1.1)$$

where

GM_j = gravitational parameter for the Moon (j=1) or the Sun (j=2)

$GM_\oplus$ = gravitational parameter for the Earth

$\hat{R}_j, R_j$ = unit vector from the geocenter to the Moon or Sun and magnitude

$\hat{r}, r$ = unit vector from the geocenter to the station and magnitude

h_2 = nominal second degree Love number (=0.609)

l_2 = nominal Shida number (=0.0852)

If the nominal values for h_2 and l_2 given above are used to compute the station displacement, only one term in the above equation needs to be corrected at the 5mm level. This is the K_1 frequency, where from Wahr's theory h_{K1} is 0.5203. Then the radial displacement is a periodic change in station height given by:

$$\delta h_{STA} = \delta h_{K_1} H_{K_1} \left(-\sqrt{\frac{5}{24\pi}} \right) 3 \sin\phi \cos\phi \sin\left(\theta_{K_1} + \lambda\right) \qquad (9.4.4.1.2)$$

where

δh_{K1} = h_{K1} (Wahr) – h_2 (nominal) = -0.0887

H_{K1} = amplitude of the K_1 term (Doodson number = 165.555) in the harmonic expansion of the tide generating potential = 0.36878 m

ϕ = geocentric latitude of the station

λ = east longitude of the station

θ_{K1} = K_1 tide argument = $\theta_g + \pi$

θ_g = Greenwich hour angle

In GEODYN, the station displacement is computed in Cartesian coordinates ΔX, ΔY, and ΔZ. Given the Cartesian components (X_j, Y_j, Z_j) and (X_{STA}, Y_{STA}, Z_{STA}) of the unit vectors $\hat{R}_j$ and $\hat{r}$ respectively, the total correction for the solid tide in the station position is:

$$\Delta X = \sum_{j=1}^{2} \left[\frac{GM_j}{GM_\oplus} \frac{r^4}{R_j^3} \right] \left\{ \left[3 l_2 \left(\hat{R}_j \cdot \hat{r} \right) \right] \hat{X}_j + \left[3 \left(\frac{h_2}{2} - l_2 \right) \left(\hat{R}_j \cdot \hat{r} \right)^2 - \frac{h_2}{2} \right] \hat{X}_{STA} \right\}$$
$$+ \delta h_{k_1} H_{k_1} \left(-\sqrt{\frac{5}{24\pi}} \right) 3 \sin\varphi \cos\varphi \sin\left(\theta_{k_1} + \lambda\right) \hat{X}_{STA} \qquad (9.4.4.1.3)$$

The expressions for ΔY and ΔZ are derived similarly.

9.4.4.2 Ocean Tide Correction

The ocean tide removal in the altimeter ocean surface height measurement is the largest of all standard corrections: in an analysis of collinear differences of sea-surface heights, [*Ray, Koblinsky, and Beckley, 1991*] found that the ocean tides were responsible for more than 80% of the signal variance. The current state-of-the art ocean tide model used by NASA GSFC is GOT4.8 [*Ray, 1999*]. Since this model is developed at GSFC, any future improvements to the model can be quickly inserted into the POD processing procedure.

The ocean tide component of the time-varying sea surface, Δh, can be represented by the following equation:

$$\Delta h(\phi,\lambda,,t) = \sum_{i=1}^{N} A_i f_i \cos\chi_i + B_i f_i \sin\chi_i$$

$$\chi_i = \omega_i t + V_i + u_i \qquad (9.4.4.2.1)$$

where

ω_i is the natural frequency of the tidal component *i*

V_i is the equilibrium argument at the origin of time *t*

ϕ is the latitude

λ is the longitude

f_i, u_i are corrections for nodal modulations of the lunar tides

A_i, B_i are the coefficients of the selected tide model

See [*Schrama and Ray, 1994*] for further discussion of the tidal height representation. The tidal height, *Δh*, is used to correct the altimeter measurement, which measures the distance from the satellite to the instantaneous sea surface, to give the distance to the mean sea surface.

9.4.4.3 Load Tide Correction

The load tide correction describes the local vertical displacement of the solid Earth underneath the ocean caused by the weight of the ocean tide. The load tide correction must therefore be consistent with the model used for the ocean tides. The load tide is here modeled as a purely elastic response to ocean loading, using a high-degree expansion in spherical harmonics (to degree and order ???). The response of each degree depends on the loading Love number h'_n; these have been adopted from the calculations by [*Farrell, 1972*]. Further detailed descriptions of this method of computing the load tide can be found in [*Ray and Sanchez, 1989*]. The magnitude of the load tide is small, with the largest amplitudes reaching 5 cm off the coast of Brazil. For the diurnal load tides, the largest amplitudes are in the northern Pacific (*e.g.* the Gulf of Alaska) and off the coast of Antarctica; in these regions the K_1 load tide reaches nearly 3 cm.

9.4.4.4 Ocean Tidal Loading

At every location on the Earth's surface, there is a local site displacement due to ocean tidal loading arising from the visco-elastic deformation of the solid Earth in response to time-varying

surface loads. The size of this correction rarely exceeds a few centimeters over the continents, and isolated islands can be affected up to 10 cm.

GEODYN applies this ocean tidal loading correction in its evaluation of tracking station locations. For each station, coefficient sets are provided characterizing the loading amplitude and phase for each tide line of importance [*Scherneck, 1996*]. These models are part of the adopted constants that are provided by IERS [*McCarthy, 1996*]. In addition to these station specific ocean loading models, it is foreseeable that laser altimetry may require regional coefficients describing these effects which are a function of local crustal thickness, distance from the ocean, and the size of regional ocean tides.

In addition to these loading time series, the coefficients of ocean tidal loading at 0.25° x 0.25° grid were computed for 36 tides using FES2012 model (Carrere et al, 2012) and using the same method. For computing the position of the bonding point, the loading displacements are computed for a 24 hour interval with step 3 hours using these coefficients. Then the field of displacement is expanded into the 3D B-spline basis, the same way is this is done for other loadings.

Scott to clean this up

9.4.4.5 Pole Tide Correction

The pole tide is the response of the ocean and the elastic Earth to variations in the centrifugal force caused by wobbling of the Earth's rotation axis. Unlike a tide, this is a tide-like effect, which occurs at other than an astronomic forcing frequency. The pole tide has two dominant frequencies: annual and 14-month, the latter being the period of the Chandler Wobble.

The pole tide correction to the altimetry is a geocentric correction, meaning that it includes both the ocean and the solid-Earth pole tide. An equilibrium response has been assumed for the ocean. An expression for the computed effect is given by [*Munk and MacDonald, 1960*].

The pole tide produces a displacement of the tracking station coordinates. GEODYN models both the altimetry correction and the displacement of tracking station coordinates as described below. The application of the pole tide in GEODYN is requested with the “POLTID” option.

Following [*Vanicek and Krakiwsky, 1982*] the displacements in r, ϕ, and λ are:

$$
\begin{aligned}
u_h &= -h_2 \frac{\omega^2 r^2}{2g} \sin 2\phi \, \delta\phi \\
u_\varphi &= -l_2 \frac{\omega^2 r^2}{g} \cos 2\phi \, \delta\phi \\
u_\lambda &= l_2 \frac{\omega^2 r^2}{g} \sin\phi \, \left(x_p \sin\lambda + y_p \cos\lambda \right) \\
\delta\phi &= \phi - \phi_0 = x_p \cos\lambda_0 - y_p \sin\lambda
\end{aligned}
\qquad (9.4.4.5.1)
$$

where h_2 and l_2 are the Love and Shida numbers defined in the previous section, and

1. = mean angular velocity of the Earth's rotation
1. = station latitude (zero subscript indicates unperturbed value)

λ = station longitude (zero subscript indicates unperturbed value)

x_p, y_p = x and y components of polar motion

g = average acceleration of gravity at the Earth's surface

r = mean Earth radius

The displacements u_ϕ, $-u_\lambda$, and u_r can be related to the local coordinate system (u, $-v$, w), and can be transformed into the geocentric Cartesian coordinate system by:

$$\begin{bmatrix} \Delta X \\ \Delta Y \\ \Delta Z \end{bmatrix} = \begin{bmatrix} -\sin\phi\cos\lambda & -\sin\lambda & \cos\phi\cos\lambda \\ -\sin\phi\sin\lambda & \cos\lambda & \cos\phi\sin\lambda \\ \cos\phi & 0 & \sin\phi \end{bmatrix} \begin{bmatrix} u_\phi \\ u_\lambda \\ u_r \end{bmatrix} \qquad (9.4.4.5.2)$$

x_p and y_p denote the position of the pole along the Greenwich and 90°E meridians, respectively. Because the pole position has a non-zero mean, which itself drifts slowly with time, a linear trend is first removed from (x_p, y_p). The (x_p, y_p) positions of the pole are obtained from the standard 5-day time series available from IERS.

The amplitude of the radial displacement is about -68.85 mm. However, when the altimeter is overflying an inland sea, not connected to the global ocean, only the solid-Earth pole tide is effective. For that case, the amplitude is scaled by the Love number factor:

$$h/(1+k) = 0.47 \qquad (9.4.4.5.3)$$

9.4.4.6 Atmospheric Loading, Continental Water Storage Loading, & Non-Tidal Ocean Loading

The crustal deformation caused by atmospheric mass loading is computed using the numerical weather model GEOS-FPIT (Rienecker et al. 2008), developed and maintained by the Goddard Modeling and Assimilation Office. The model has resolution 0.625° x 0.5° x 72 layers x 3 hours, runs from 2000.01.01 through presents, updated 4 times a day and has latency 10-15 hours. The output of the numerical weather model among other parameters contains thickness of atmospheric layers, air temperature, and specific humidity at each grid point. The atmospheric pressure is computed for every grid point by solving the hypsometric differential equation. Then the air pressure is re-gridded to the finer D1023 grid (0.088° x 0.088° x 72 layers 3 hours) and interpolated to the surface. The surface pressure at the D1023 grid is multiplied by the see/land mask and expanded into spherical harmonics of degree/order 1023. The harmonics are scaled by

the factor that depends on degree and the appropriate Love number computed for the PREM model. Then the scaled spherical harmonics are underwent to the inverse vector spherical harmonics transform degree/order 1023. The results of the operation is the 3D field of deformations caused by the atmospheric pressure loading at a grid 0.088deg x 0.088deg x 3 hours. For reducing storage space, the resolution is truncated to D359 (0.25° x 0.25°). In order to compute the displacement of the bouncing point due to the loading, the displacement field is expanded into the 3D tensor products of B-splines for a 24 hour interval of time. The coefficients of expansion are used for computing the loading displacement at a given a priori position of the bouncing point and given moment of time.

In a similar way, the crustal deformations caused by the continental water storage and non-tidal variations of the ocean bottom pressure are computed. TWLAND data product (Reichle, 2011) provided by the GEOS-FPIT model represents the surface pressure of water that is contained in snow and soil. The resolution and latency of GEOS-FPIT TWLAND product is the same as for the atmospheric products: 0.625° x 0.5° x 3 hours. The field of ocean bottom pressure with tides removed is derived from the AOD1B product computed using the OMCT model (Thomas, 2002; Dobslaw & Thomas, 2007) by the GFZ. The AOD1B product is a set of Stokes coefficients of the contribution of the ocean bottom pressure anomaly to gravity truncated to degree/order 100. An iterative procedure restores the bottom pressure and mitigates the distortion caused by truncation of Stokes coefficients in AOD1B. It involves the inverse spherical harmonics transform of AOD1B, upgridding to degree/order 1023, and zeroing the ocean bottom pressure at land. The result of this procedure is the ocean bottom pressure that is used for loading computation. The AOD1B products have time step 6 hours and latency 20-50 days.

The atmospheric, land-water storage and ocean non-tidal loadings are computed independently by two servers of the International Mass Loading Service http://massloading.net and http://alt.massloading.net. For better reliability, the servers are located in different locations 10 miles away and connected to different networks. The servers provide the time series of mass loadings at the global grid with resolution 0.25° x 0.25° with a delay not exceeding 2 hours upon availability the output of atmospheric, hydrology and ocean models.

9.4.4.7 Earth Center of Mass and Orientation Parameters

To first approximation, the rotational transformations involving precession, nutation, the rotation of the Earth, and the motion of the pole represented by polar motion define the transformation between the celestial and terrestrial reference frames. Also, it is assumed that the location of the center of mass of the Earth and the origin of the terrestrial coordinate system (as defined by the coordinates of the global network of tracking stations) coincide.

When the time-dependent motions of masses on the Earth, mostly due to tides, are considered, the above picture must be modified. The inertial coordinate system of the satellite orbit is defined relative to the center of mass of the Earth. The origin of the terrestrial coordinate system

(*i.e.* the geometrical center) is defined by the coordinates of the global network of tracking stations. When mass moves in or on the Earth, the geometrical center will move relative to the center of mass of the Earth.

In order to account for the component of this motion, which is due to earth and ocean tides, GEODYN allows modification of site positions and earth orientation parameters at the tidal frequencies. See Section ??? for a discussion of tidal frequencies.

The motion of the geometrical center relative to the center of mass is accounted for by applying displacements in x, y and z of the Earth-centered coordinates of the sites. Each of these displacements is represented as a sinusoid, with a frequency specified as one of the tidal frequencies, and a freely adjustable amplitude and phase.

The perturbations to the rotation of the Earth caused by the tidal motions are represented as time-varying components of the A1-UT1 time difference, and of the x and y coordinates of the pole. These components are also sinusoids of the tidal frequencies, and have adjustable amplitudes and phases.

A review of this topic can be found in [*Chao and Ray, 1997*].

9.4.5 Observation Corrections

9.4.5.1 Offsets

The offsets considered in satellite orbit determination refer, in general, to the corrections that must be applied in the spacecraft body-fixed coordinate system to relate the location of the center of mass of the satellite to the location of the antennae or tracking instruments. The orbit determination process computes the position of the center of mass of the satellite, while the tracking systems measure the distances between the tracking instruments. The offsets supply the link between these processes, and differ for the different tracking systems.

For satellite laser ranging, two types of offsets must be accounted for: (1) the offset of the laser retro-reflector from the center of mass of the satellite, and (2) the offsets in the laser and the receiving telescope.

GEODYN can apply a laser retro-reflector offset given in terms of distances in X, Y and Z in the satellite body-fixed coordinate system. The program computes the projection of this vector in the direction of the laser beam and applies this projection to correct the laser range to be the range to the center of mass. The offsets in the laser and receiving telescope are applied in the laser data preprocessing.

The GPS antenna locations are modeled with offsets in the spacecraft body-fixed system, and the geometry provided by the GPS measurements enables the estimation of both X and Z-axis antenna offsets. In addition, corrections such as pass-by-pass ambiguity biases, and GPS receiver time tag errors are estimated for the GPS data.

9.4.5.2 Tropospheric and Ionospheric Propagation Delay

Satellite laser range measurements must be corrected for the propagation delay caused by the atmosphere medium. Atmospheric refraction at optical wavelengths is commonly treated as two separate components, a dry and wet term. The dry tropospheric correction requires the barometric surface pressure at the tracking site. The wet tropospheric correction term is caused by the delay of the signal due to refraction through atmospheric water vapor and cloud liquid water, and seldom exceeds 1 cm for laser tracking.

SLR tracking stations often measure the local pressure, temperature, and relative humidity data needed to compute the tropospheric corrections. When such data are not included in the measurement record, GEODYN uses corrections based on standard meteorological values appropriate to the station height above sea level.

GEODYN applies the classic model developed by [*Marini and Murray, 1973*] to compute the refraction path delay incurred through refractive bending for the SLR measurements. This range correction takes the form:

$$\Delta R = \frac{f(\lambda)}{f(\phi,H)} \frac{(A+B)}{\sin E + \dfrac{B/(A+B)}{\sin E + 0.01}} \approx 2.1\, meters\ (at\ 90^{\circ}) \qquad (9.4.5.2.1)$$

where

$$A = 0.002357P + 0.000141e$$

$$B = (1.084\times10^{-8})PTK + (4.734\times10^{-8})(P^2/T^2)\left[2/(3-1/k)\right]$$

$$K = 1.163 - 0.00968\cos(2\phi) - 0.00104T + 0.00001435P$$

$$f(\phi,H) = 1 - 0.0026\cos(2\phi) - 0.00031H$$

$$f(\lambda) = 0.9650 + \frac{0.0164}{\lambda^2} + \frac{0.000228}{\lambda^4}$$

$$e = \frac{R_h}{100} \times 6.11 \times 10^{\left[\frac{7.5(T-273.15)}{237.3+(T-273.15)}\right]}$$

R_h is the relative humidity

E is the elevation of the ray path

P is the atmospheric surface pressure (mbar)

T is the surface temperature (K)

λ is wavelength of light

H is surface height

ϕ is latitude of surface point

Computation of slant path delay through the neutral atmosphere is performed by three procedures. The first procedure, data acquisition is performed by the designated server. The server downloads the numerical weather model GEOS-FPIT (Rienecker et al. 2008) developed and maintained by the Goddard Modeling and Assimilation Office. The model has resolution 0.625 x 0.5 deg x 72 layers x 3 hours, runs from 2000.01.01 through presents, updated 4 times a day and has latency 10-15 hours. The output of the numerical weather model among other parameters contains thickness of atmospheric layers, air temperature, and specific humidity at each grid point. These parameters are used for computing refractivities at three wavelength ranges: 532nm, 1064 nm, and 1mm-30m (radio). The refractivity accounts for both dry air and water vapor. The data acquisition procedure stores for each epoch 3D refractivity field at a regular grid with the height range from -1000, to 80000 km above the reference ellipsoid. The data acquisition procedure runs every hour and check whether the new output from the GEOS-FPIT model become available.

The second procedure computes slant path delay for a designated set of stations. The path delay is computed on a regular, but non-uniform grid over azimuth and elevation. For each station, each epoch, each direction the trajectory of the wavefront is computed by solving a system of non-liner differential equations of the 4th order that are the solution of the variational problem of wave propagation in accordance with the Fermat principle. Then the path delay is computed by integrating the refractivity along the trajectory from the receiver (i.e. observing station) to the top of the atmosphere defined at the height of 80 km. All slant path delay for all directions, all stations for a given epochs are stored in an output file. Path delays for designated "continuous" stations are computed immediately after completion of the data acquisition procedure.

The third procedure is incorporated into a space geodesy data reduction software, such as GEODYN and Calc/Solve. The procedure determines the time range of observations and the list of stations. It downloads files with slant path delay on an azimuth-elevation grid. For each station it expands the path delay over the tensor product of the 3D B-spline basis that runs over azimuth, elevation, and time. Then, using these expansion coefficients, slant path delay and its partial derivatives with respect to the path delay in zenith direction are computed to a given moment of time, given elevation and azimuth of the geodetic observation.

SLR measurements are not significantly affected by ionospheric delay, and no correction is applied. Ionospheric delays do affect the ground to GPS segment of the GPS observation, and may affect the user satellite to GPS segment, depending on the user satellite altitude. The ionospheric delay can be eliminated, by combining the L1 and L2 frequencies of the GPS signal.

The ionospheric model based on the IRI-95 model [*Bilitza et al., 1995*] has been implemented in GEODYN and will be used for ionospheric corrections to ICESat-2 GPS measurements.

9.4.5.3 Relativistic Effects

The two-way SLR measurements have no need for corrections for relativistic effects. However, the GPS measurement depends on satellite and ground station clocks and so the relativistic effects on the satellite clocks must be computed.

GEODYN has the capability of correcting satellite clocks for relativistic effects. There are two relativistic effects to be considered: (1) a secular difference from ground clocks due to the different geopotential frame of the satellite clock at its mean altitude, and due to its mean velocity, and (2) a periodic effect due to variations in the satellite altitude and velocity caused by the eccentricity of its orbit. GPS satellite clocks have been corrected for effect (1) and no additional correction is needed, while ICESat-2 clocks must account for the effects of both (1) and (2).

Following [*Soffel, 1989*], the general clock correction for satellite clocks is:

$$\rho_{corr} = -\frac{1}{c}\left(\frac{GM}{r_{STA}} + \frac{1}{2}\Omega^2\left(x_{STA}^2 + y_{STA}^2\right) - \frac{3}{2}\frac{GM}{a}\right)\tau_{(e)} + \frac{2}{c}\left(\vec{x}_S \cdot \vec{v}_S\right) \qquad (9.4.5.3.1)$$

where

$\tau_{(e)}$	is the (time the signal was emitted) – (time of clock synchronization)
r_{STA}	is the magnitude of the station position vector
x_{STA}, y_{STA}	are the *x* and *y* components of the station position vector
Ω	is the rotation rate of the Earth
a	is the semi-major axis of the satellite orbit
$\vec{x}_S, \vec{y}_S$	are the satellite position and velocity in geocentric coordinates

For GPS satellites, the clock range correction is simply:

$$\rho_{corr} = \frac{2}{c}\left(\vec{x}_S \cdot \vec{v}_S\right) \qquad (9.4.5.3.2)$$

REFERENCES

Andersen, O. B., "The DTU10 Gravity field and Mean Sea Surface," Second international symposium of the gravity field of the Earth (IGFS2), Fairbanks, Alaska, 2010.

Barlier, F., C. Berger, J.L. Falin, G. Kockarts, and G. Thuillier, A Thermospheric Model Based on Satellite Drag Data, Institut d'Aeronimic Spatiale de Belgique, Aeronomica Acta, 1977.

Bilitza, D., C. Koblinsky, B. Beckley, S. Zia, and R. Williamson, "Using IRI for the computation of ionospheric corrections for altimeter data analysis", Adv. Space Res., 15, 2, pp. 113-119, 1995.

Carrere L., F. Lyard, M. Cancet, A. Guillot, L. Roblou, FES2012: A new global tidal model taking taking advantage of nearly 20 years of altimetry, Proceedings of meeting "20 Years of Altimetry", Venice 2012.

Cartwright and Edden, Geophys. J. Roy. Astron. Soc., 33, 253-264, 1973.

Chao, B. F. and R. D. Ray, "Oceanic tidal angular momentum and Earth's rotation variations", Prog. Oceanog., Vol. 40, pp. 399-421, 1997.

Christodoulidis, D.C., Smith, D.E., Klosko, S.M. and Williamson, R.G., "Observed Tidal Braking in the Earth/Moon/Sun System", J. Geophys. Res., Vol. 93, B6, pp. 6216-6236, 1988.

Colombo, O. L., "Altimetry, Orbits and Tides," NASA Tech. Memo. 86180, Nov. 1984.

Coppola, V. T., Seago, J. H., Vallado, D. A., "The IAU 2000a and IAU 2006 Precession-nutation Theories and Their Implimentation." American Astronautical Society. 2009.

Diamante, J. M. and R. G. Williamson, "Error Models for Solid Earth and Ocean Tidal Effects in Satellite Systems Analysis", Wolf Research and Development Corp., Contract No. NAS 5-11735 mod 57 for NASA Goddard Space Flight Center, 1972.

Dobslaw, H., Thomas, M., Simulation and observation of global ocean mass anomalies, jgr, 112, C05040, 2007.

Farrell, Reviews of Geophysics and Space Physics, 10, 761-797, 1972.

Gill, A., Atmosphere-Ocean Dynamics, Academic Press, 1982.

Goad C. C., L. Goodman, "A modified Hopfield tropospheric refraction correction model," American Geophysical Union Annual Fall Meeting, San Francisco, Dec. 12-17, 1974.

[Gross, 1984] ?

Gross, R. S., "A combination of Earth orientation data: Space93", IERS Annual Report, Observatory of Paris, 1993.

Guinot, B., "Report of the Sub-group on Time", in Reference Systems, J. A. Hughes, C. A. Smith, and G. H. Kaplan (eds.), U. S. Naval Observatory, Washington, D. C., 3-16, 1991.

Hedin, A., "MSIS-86 Thermospheric Model", J. Geophys. Res., Vol. 92, No. A5, 4649-4662, 1987.

Hofmann-Wellenhof, B., H. Lichtenegger, and J. Collins, GPS: Theory and Practice, Third Edition, Springer-Verlag, Wien, 1994.

Huang, C., J. C. Ries, and M. M. Watkins, "Relativistic Effects for Near Earth Satellite Orbit Determination, Celestial Mechanics and Dynamical Astronomy, Vol. 48, 167-185, 1990.

Ivins ER, James TS, Wahr J, Schrama EJO, Landerer FW and Simon KM (2013) Antarctic.

Knocke, P.C., J.C. Ries, B.D. Tapley, Earth Radiation Pressure Effects on Satellites, Proceedings of the AIAA/AAS Astrodynamics Conference, 577–586, 1988.

Koblinsky, C. J., B. D. Beckley, R. D. Ray, Y. M. Wang, L. Tsaoussi, A. Brenner, R.Williamson, NASA Ocean Altimeter Pathfinder Project, Report 1, National Aeronautics and Space Administration, 1998.

Kouba, J., "A simplified yaw-attitude model for eclipsing GPS satellites", GPS Solut (2009) 13:1–12 DOI 10.1007/s10291-008-0092-1

Lambeck, K., The Earth's variable rotation: Geophysical causes and consequences, Cambridge Univ. Press, 1980.

Le Provost et al, J. Geophys. Res., 99, 24777, 1994.

Lemoine, F. G., S. C. Kenyon, J. K. Factor, and R. G. Trimmer, N. K. Pavlis, D. S. Chinn, C. M. Cox, S. M. Klosko, S. B. Luthcke, M. H. Torrence, Y. M. Wang, and R. G. Williamson, E. C. Pavlis, R. H. Rapp, and T. R. Olson, "The Development of the Joint NASA GSFC and NIMA Geopotential Model EGM96," NASA/GSFC, 1996.

Lemoine, F.G., Zelensky N.P., Chinn, D.S., Pavlis, D.E., Rowlands, D.D., Beckley, B.D., Luthcke, S.B., Willis, P., Ziebart, M., Sibthorpe, A., Boy, J.P., Luceri, V., (2010) Towards development of a consistent orbit series for TOPEX/Poseidon, Jason-1, and Jason-2, Adv. in Space Research, doi:10.1016/j.asr.2010.05.007.

Lieske, J. H., T. Lederle, W. Fricke, and B. Morando, "Expression for the Precession Quantities Based upon the IAU (1976) System of Astronomical Constants", Astron. Astrophys, 58, 1-16., 1977.

Luthcke, S.B. , Marshall, J.A., Rowton, S.C., Rachlin, K.E. and Cox, C.M. (1997), Enhanced Radiative Force Modeling of The Tracking and Data Relay Satellites, Journal of Astronautical Sciences, Vol. 45, No. 3, July-September, pp. 349-370.

Luthcke, S.B., D.D. Rowlands, T.A. Williams, M. Sirota,"Reduction of ICESat systematic geolocation errors and the impact on ice sheet elevation change detection," Geophys. Res. Lett., 32, L21S05, doi:10.1029/2005GL023689, 2005.

Luthcke, S. B., N. P. Zelensky, D. D. Rowlands, F. G. Lemoine, T. A. Williams, "The 1-Centimeter Orbit: Jason-1 Precision Orbit Determination Using GPS, SLR, DORIS, and Altimeter Data," Marine Geodesy, Special Issue on Jason-1 Calibration/Validation, Part 1, Vol. 26, No. 3-4, pp. 399-421.

Luthcke, S.B., C.C. Carabajal and D.D. Rowlands, Enhanced geolocation of spaceborne laser altimeter surface returns: parameter calibration from the simultaneious reduction of altimeter range and navigation tracking data," Journal of Geodynamics, Vol. 34, No. 3-4, October/November, pp. 447-475, 2002.

Luthcke, S.B., D.D. Rowlands, J.J. McCarthy, E. Stoneking and D.E. Pavlis, Spaceborne Laser Altimeter Pointing Bias Calibration From Range Residual Analysis, Journal of Spacecraft and Rockets, Vol. 37, No. 3, May-June, pp. 374-384, 2000.

Luthcke, S. B., J. A. Marshall, "Nonconservative Force Model Parameter Estimation Strategy for TOPEX/Poseidon Precision Orbit Determionation," NASA Technical Memorandum 104575, 1992.

Marshall, J.A. and S.B. Luthcke, (1994) "Nonconservative Force Model Performance for TOPEX/Poseidon Precision Orbit Determination," Journal of Astronautical Sciences, Vol. 41, No. 2, April-June, pp. 229-246.

Marini, J. W. and C. W. Murray, Jr., "Correction of Laser Range Tracking Data for Atmospheric Refraction at Elevations above 10 Degrees", NASA/GSFC Report X-591-73-351, 1973.

McCarthy, D. D., IERS Technical Note 21, July 1996.

McCarthy, J. J., T. V. Martin, "A Computer Efficient Model of Earth Albedo Satellite Effects", NASA Goddard Space Flight Center, Planetary Sciences Dept. Report No. 012-77, 1977.

Mueller, I. I., Spherical and Practical Astronomy as applied to Geodesy, F. Ungar Publishing Co., 1969.

Munk, W., D.E. Cartwright, Philosophical Transactions of the Royal Society, A259, 533-581, 1966.

Nerem, R S, B Putney, J A Marshall, F Lerch, E Pavlis, S Klosko, S Luthcke, G Patel, R Williamson, N Zelensky, IEEE Transactions on Geoscience and Remote Sensing, 31, 333-354, 1993.

Paulson A, Zhong S and Wahr J (2007) Inference of mantle viscosity from GRACE and relative sea level data. Geophys. J. Int., 171(2), 497–508 (doi: 10.1111/j.1365-246X.2007.03556.x)

Pavlis, D. E., D. Moore, S. Luo, J. J. McCarthy, S. B. Luthcke, GEODYN Operations Manual, 5 volumes, Raytheon STX Corporation, 1998.

Peltier WR (2004) Global glacial isostatic adjustment and the surface of the ice-age Earth: the ICE-5G(VM2) model and GRACE. Annu. Rev. Earth Planet. Sci., 32, 111–149 (doi: 10.1146/annurev.earth.32.082503.144359)

Petit, G. and B. Luzum, 2010, "IERS Conventions (2010)," IERS Technical Note No. 36, International Earth Rotation and Reference System Service (IERS).

Pie, Nadege, "Design Concepts for Repeat Groundtrack Orbits and Application to the ICESat Mission", *Dissertation – The University of Texas at Austin*, 2008.

Ray, R. D., "A global ocean tide model from TOPEX/POSEIDON altimetry: GOT99.2," NASA Tech. Memorandum 1999-209478, Goddard Space Flight Center, Greenbelt, MD, 1999.

Ray, R.D., C J Koblinsky, B D Beckley, International Journal of Remote Sensing, Vol. 12, no. 9, 1979-1984, 1991.

Ray, R.D, and B. Sanchez, "Radial Deformation of the Earth by Oceanic Tidal Loading", NASA Technical Memorandum 100743, 49 pp., July 1989.

Ray RD (1999) A global ocean tide model from TOPEX/Poseidon altimetry/GOT99.2. (NASA Tech. Rep. NASA/TM-1999-209478) NASA Goddard Space Flight Center, Greenbelt, MD

Reichle, R.H., Koster, R.D, De Lannoy, G.J.M., Forman, B.A., Liu, Q., Mahanama, S.P.P, Toure, A., Assessment and Enhancement of MERRA Land Surface Hydrology Estimates, J. Climate, 24, 6322--6338, 2011.

Rienecker, M.M., Suarez, M.J., Todling, R., Bacmeister, J., Takacs, L., Liu, H.C., Sienkiewicz, W.M., Koster, R.D., Gelaro, R., Stajner I., and Nielsen E., ``The GEOS Data Assimilation System --- Documentation of Versions 5.0.1, 5.1.0, and 5.2.0.", NASA/TM--2008--104606, 2008. http://gmao.gsfc.nasa.gov/pubs/docs/tm27.pdf

Ries, J. C., S. Bettadpur, S. Poole, T. Richter, "Mean Background Gravity Fields for GRACE Processing," GRACE Science Team Meeting, Austin, TX, 8-10 August 2011.

Rodriguez-Solano, C. J., U. Hugentobler, P. Steigenberger, "Adjustable box-wing model for solar radiation pressure impacting GPS satellites", Advances in Space Research", 2012 ("gps- BoxWing_TUM_asr12.pdf ")

Rodriguez-Solano, C. J., Masters Thesis, TUM, 2009 ("albedo gps.Master.Thesis.Rodrigez_Solano_MS09.pdf ".)

Roh, K-M. et al., "Investigating suitable orbits for the SWARM constellation mission – The frozen orbit", *Aerospace Science and Technology*, 13, 49-58, 2009.

Rowlands, D.D., D.E. Pavlis, F.G. Lemoine, G.A. Neuman and S.B. Luthcke, "The use of laser altimetry in the orbit and attitude determination of mars global surveyor," Geophys. Res. Lett., 26, No. 9, 1191-1194, 1999.

Rowlands, D. D., S. B. Luthcke, J. A. Marshall, C. M. Cox, R. G. Williamson, and S. C. Rowton, "Space Shuttle Precision Orbit Determination in Support of SLA-1, Using TDRSS and GPS Tracking Data", J. Astronaut. Sci., Vol. 45, No. 1, 113-129, January/March 1997.

Saastamoinen, J., "Atmospheric correction for the troposphere and stratosphere in radio ranging of satellites", Geophysical Monograph 15, American Geophysical Union, 1972.

Scherneck, H.G., "Site displacement due to ocean loading," McCarthy D.D.(editor): IERS Technical Note 21, 52-56, 1996.

Schrama, E.J.O., and R.D. Ray, J. Geophys. Res., 99, 24799, 1994.

Seidelmann, P. K., "1980 IAU Nutation: The Final Report of the IAU Working Group on Nutation", Celestial Mechanics, 27, pp. 79-106, 1982.

Shum et al. (J. Geophys. Res., in press, 1996).

Soffel, Relativity in astrometry, celestial mechanics, and geodesy, Springer-Verlag, New York, 1989.

Standish, E. M., Newhall X X, Williams, J. G. and Folkner, W. F., 1995, "JPL Planetary and Lunar Ephemerides, DE403/LE403", JPL IOM 314.10-127, 1995.

Taff, L., Celestial Mechanics, John Wiley & Sons, New York, 1985.

Tapley, B., B. Schutz, G. Born, Statistical Orbit Determination, Elsevier Academic Press, Burlington, MA, 2004.

Thomas, M., Ozeanisch induzierte Erdrotationsschwankungen Ph. D. Thesis, 2002.

Vallado, David A., "Fundamentals of Astrodynamics and Applications Second Edition", 9.6, 606-608, 2001.

Vanicek, P. and E. J. Krakiwsky, Geodesy: the Concepts, Section 25.4, North-Holland Publishing Co., 1982.

Wahr, J., "Body Tides on an Elliptical, Rotating, Elastic and Oceanless Earth," Geophys. J. Roy. Astron. Soc., 64, 677-703, 1981.

Wahr, J. M., "The Forced Nutation of an Elliptical, Rotating, Elastic and Oceanless Earth", Geophys. J. Roy. Astron. Soc., 64, 705-727, 1981.